Received: 21 July 2023 | Revised: 21 September 2023 | Accepted: 26 September 2023

DOI: 10.1111/mmi.15181

RESEARCH ARTICLE

WILEY

RNase III participates in control of quorum sensing, pigmentation and oxidative stress resistance in *Rhodobacter sphaeroides*

Janek Börner [1] | Tobias Friedrich [2,3] | Gabriele Klug [1]

[1]Institute of Microbiology and Molecular Biology, Justus-Liebig-University Giessen, Giessen, Germany

[2]Biomedical Informatics and Systems Medicine, Justus-Liebig-University Giessen, Giessen, Germany

[3]Institute of Biochemistry, Justus-Liebig-University Giessen, Giessen, Germany

Correspondence
Gabriele Klug, Institute of Microbiology and Molecular Biology, Justus-Liebig-University Giessen, Heinrich-Buff-Ring 26-32, Giessen 35392, Germany.
Email: gabriele.klug@mikro.bio.uni-giessen.de

Funding information
Deutsche Forschungsgemeinschaft, Grant/Award Number: Kl563/41-1

Abstract

RNase III is a dsRNA-specific endoribonuclease, highly conserved in bacteria and eukarya. In this study, we analysed the effects of inactivation of RNase III on the transcriptome and the phenotype of the facultative phototrophic α-proteobacterium *Rhodobacter sphaeroides*. RNA-seq revealed an unexpectedly high amount of genes with increased expression located directly downstream to the rRNA operons. Chromosomal insertion of additional transcription terminators restored wild type-like expression of the downstream genes, indicating that RNase III may modulate the rRNA transcription termination in *R. sphaeroides*. Furthermore, we identified RNase III as a major regulator of quorum-sensing autoinducer synthesis in *R. sphaeroides*. It negatively controls the expression of the autoinducer synthase CerI by reducing *cerI* mRNA stability. In addition, RNase III inactivation caused altered resistance against oxidative stress and impaired formation of photosynthetically active pigment-protein complexes. We also observed an increase in the CcsR small RNAs that were previously shown to promote resistance to oxidative stress. Taken together, our data present interesting insights into RNase III-mediated regulation and expand the knowledge on the function of this important enzyme in bacteria.

KEYWORDS
bacterial photosynthesis, quorum sensing, *Rhodobacter*, riboregulation, RNase III, stress response

1 | INTRODUCTION

For many years, it was assumed that in bacteria regulation of gene expression occurs nearly exclusively on the levels of transcription and translation, however, the last decades have unveiled the crucial role of riboregulation. Riboregulation describes the action of ribonucleases, noncoding regulatory RNAs and RNA-binding proteins that often influence gene expression by stabilisation or destabilisation of messenger RNAs, which consequently affects the translatome and thereby the proteome. Bacteria use riboregulation to quickly and cost-efficiently adapt gene expression to changing environmental conditions, which is reflected by generally much shorter RNA half-lives (often in a range of minutes) in bacteria, compared to eukaryotes (often in a range of hours) (Belasco & Brawerman, 1993).

While being first discovered in *Escherichia coli* in 1967 (Robertson et al., 1967, 1968), RNase III was intensely studied in

the following years for its ability to specifically cleave double-stranded RNA (dsRNA) substrates. The physiological functions of RNase III were described mainly in the maturation of the ribosomal RNA (Dunn & Studier, 1973; Nikolaev et al., 1973) and processing of viral RNA (Westphal & Crouch, 1975). In many α-proteobacteria, RNase III is also responsible for the fragmentation of the 23S rRNA (Evguenieva-Hackenberg & Klug, 2000). Genome-sequencing approaches revealed that the enzyme is highly conserved not only in bacteria, but homologues are present in nearly every living organism, except of many archaeal species (Nicholson, 2014). Prokaryotic members of the RNase III family have a simple architecture, often only consisting of a catalytically active C-terminal RNase III Domain (RIIID) and an N-terminal dsRNA binding domain. Eukaryotic members of the RNase III family can possess two RIIID (Drosha and Dicer) and additionally, a helicase and a PAZ (Piwi Argonaute Zwille) domain (Dicer), which are used to establish RNA–RNA interactions for gene silencing via RNA interference (Carmell & Hannon, 2004; Court et al., 2013; Kang & Hata, 2012).

A well-studied example of the direct action of RNase III on mRNAs is the processing of the *pnp* transcript in many bacteria (Carzaniga et al., 2009; Gatewood et al., 2011; Portier et al., 1987; Régnier & Grunberg-Manago, 1990; Snow et al., 2020). The *pnp* mRNA encodes the polynucleotide phosphorylase (PNPase), an important exoribonuclease with 3′ to 5′ phosphorolytic activity. As a primary transcript *pnp* harbours a stabilising 5′ RNA structure and is highly stable resulting in frequent translation. However, degradation of the *pnp* transcript is initiated through recognition of the 5′ RNA structure by RNase III and followed by dsRNA cleavage. Subsequently, one strand of the opened 5′ double-strand structure is removed by PNPase, resulting in a single-stranded 5′ end region of *pnp* accessible for RNase E-mediated degradation.

In particular, the development of low-cost high throughput RNA sequencing (RNA-seq) methods in the beginning of the early 2000s and its applications revealed new functions of RNase III. RNase III was previously known to primarily affect maturation of ribosomal and transfer RNAs, but the spectrum of other RNAs recognised by RNase III has been largely expanded in the last decades (Altuvia et al., 2018; Gatewood et al., 2012; Ifill et al., 2021; Rath et al., 2017).

Moreover, the discovery of a variety of novel regulatory non-coding RNAs through RNA-seq has rekindled interest in RNase III. Non-coding regulatory RNAs are part of the riboregulation network and were not only described in bacteria (in bacteria called sRNAs) but also in numerous other organisms (reviewed in Jørgensen et al., 2020; Mahendran et al., 2022; Papenfort & Melamed, 2023; Storz et al., 2011). sRNAs can exert their regulatory effects on gene expression by specific base pairing with their target mRNAs, and thereby form RNA–RNA duplexes, which are often recognised by RNase III as a substrate (Lioliou et al., 2012; McKellar et al., 2022; Mediati et al., 2022). While a direct action of RNase III in sRNA-mediated regulation of plasmid copy numbers was already described quite early (Blomberg et al., 1990; Conrad & Campbell, 1979), other established functions of RNase III acting on sRNA-mediated regulation were found in regulation of type I toxin-antitoxin systems (Gerdes et al., 1992; Vogel et al., 2004), stress responses (Afonyushkin et al., 2005; Lalaouna et al., 2019; Opdyke et al., 2011) or virulence of pathogenic bacteria (Boisset et al., 2007; Huntzinger et al., 2005; Romby et al., 2006).

We discovered several small regulatory RNAs (sRNAs) (Berghoff et al., 2009), which affect important physiological processes like, for example, growth and cell division (Grützner, Remes, et al., 2021), stress resistance (Adnan et al., 2015; Billenkamp et al., 2015; Müller et al., 2016; Peng et al., 2016) and formation of photosynthesis complexes (Eisenhardt et al., 2018; Mank et al., 2012; Reuscher & Klug, 2021) in the model organism *Rhodobacter sphaeroides* (recently renamed to *Cereibacter sphaeroides*, Hördt et al., 2020). *R. sphaeroides* is a gram-negative purple non-sulphur bacterium with versatile metabolism, able to live under a variety of different environmental conditions, which makes it a well-suited model to study adjustment of gene expression to changing environmental conditions.

To investigate the functional role of RNase III in *R. sphaeroides*, especially its impact on regulation of gene expression, we inactivated the catalytic activity of RNase III by exchanging two highly conserved amino acids (G48S, D49R) within the active centre of the native enzyme. An obvious effect of the RNase III deficiency was pronounced in a drastically reduced photopigment production. Moreover, we could observe increased cell survival rates of the mutant upon oxidative stress exposure, which are accompanied by elevated expression of CcsR sRNAs, which counteract oxidative stress through negative regulation of a glutathione-dependent metabolic pathway, leading to accumulation of antioxidative glutathione. Strikingly, we found a novel regulatory function of RNase III in the quorum-sensing system of *R. sphaeroides*, where RNase III negatively controls the expression of the quorum-sensing autoinducer synthase (*cerI*) by mRNA destabilisation, consequently resulting in reduced autoinducer production. Interestingly, lack of RNase III activity does not only affect 23S rRNA fragmentation but also transcript levels of genes located downstream of the three rRNA operons.

2 | RESULTS

2.1 | Inactivation of the *R. sphaeroides* RNase III leads to strong decrease in pigmentation

Like in the well-studied γ-proteobacterium *E. coli*, the RNase III encoding gene (*rnc*) in *R. sphaeroides* is chromosomally organised in an operon consisting of three genes, giving rise to a polycistronic mRNA. While in *E. coli*, the *rnc* gene is the first gene of the operon, followed by the *era* gene (encoding a GTPase important for cell cycle control) and the *recO* gene (encoding a DNA repair protein), in *Rhodobacter* the first gene is *lep* for leader peptidase, followed by the *rnc* gene and the *era* gene on last position (Rauhut et al., 1996).

In the first approach, we constructed an *R. sphaeroides rnc* deletion mutant (Δ*rnc*), by substitution of the native *R. sphaeroides* gene with a kanamycin resistance cassette, leading to loss of RNase III activity but also showing polar effects of the mutation. A strong phenotype was visible in a drastic filamentation morphology of the Δ*rnc*-mutant stain, which we could attribute to a reduced *era* mRNA

level in the mutant. To exclude polar effects, we next inactivated RNase III catalytic activity through the exchange of two highly conserved amino acids (G48S, D49R) within the RIIID signature motif (Figure S1). This approach relies on mutations described in previous studies (Apirion & Watson, 1975; Dasgupta et al., 1998; Kindler et al., 1973; Nashimoto & Uchida, 1985) and was adapted in our study to the *R. sphaeroides* RNase III enzyme.

To test for loss of RNase III activity, we checked the ability of the *R. sphaeroides* enzyme to fragment ribosomal RNAs. Like several other α-proteobacteria, *R. sphaeroides* fragments the large 23S rRNA into smaller pieces, thereby generating a 14S, 5.8S-like and an additional 16S rRNA molecule (Evguenieva-Hackenberg, 2005; Evguenieva-Hackenberg & Klug, 2000; Zahn et al., 2000). This process is strictly RNase III-dependent in *R. sphaeroides*. To analyse the rRNA expression pattern of the mutated cells, generated by the exchange of the two mentioned amino acids (Figure S1), we isolated and visualised total RNA by gel electrophoresis and ethidium bromide staining (Figure S2). The presence of intact 23S rRNA and the absence of 14S and 5.8S-like rRNA fragments in total RNA of the mutated cells (*rnc*_GD48,49SR; from now referred to as *rnc*$^-$ strain) confirmed the inactivity of RNase III. As a control, we constructed a plasmid (pRK-*rnc*) harbouring a copy of the native *rnc* gene under transcriptional control of the native promoter and transferred it to the *rnc*$^-$ cells by diparental conjugation (complementation strain). Analysis of the rRNAs from total RNA samples of the complementation strain revealed the restoration of a wild type-like cleavage pattern, indicating that the loss of RNase III can be complemented by ectopic expression of the native *rnc* gene (Figure S2). Band intensities showed some variation between the complemented strain and the wild type and an additional band occurred in the complemented strain. This may be due to different RNase levels in the two strains caused by expression from the pRK vector. Only the wild type and *rnc* mutant were used in our further analyses.

To analyse the growth behaviour of the *rnc*$^-$ strain in comparison to the wild type, we cultivated both strains under aerobic (high oxygen tension), microaerobic (low oxygen tension) or phototrophic conditions (anaerobic, illuminated with white light) in malate minimal medium and followed the OD_{660} over a time of 35 h (Figure 1). While in the presence of oxygen *R. sphaeroides* performs chemotrophic growth through aerobic respiration, photosynthesis is used for energy conservation in the absence of oxygen and the presence of light (phototrophic conditions). As a result, only a minor growth deficiency of the mutant was visible under aerobic and phototrophic conditions, while under microaerobic conditions, the growth of mutant and wild type was similar.

During the growth analyses, we observed a paler colour of the mutant cultures as an obvious phenotype. Since the colour of *R. sphaeroides* cultures is defined by their type and degree of pigmentation, we analysed the production of photopigments. For this, we first performed a spectral analysis of both strains grown in a minimal medium under microaerobic or phototrophic growth conditions (Figure 2a). The spectra of the mutant showed a strongly decreased absorbance at wavelengths, where carotenoids and bacteriochlorophyll possess specific absorbance maxima. The photosynthetic apparatus of *R. sphaeroides* comprises the reaction centre (RC) and two light-harvesting complexes (LHI and LHII). The reduced absorbance at these specific wavelengths was more pronounced under microaerobic growth conditions.

Next, we extracted the photopigments of both strains via acetone/methanol extraction (Figure 2b). The measured amounts of extracted pigments confirmed our expectations, indicating that the *rnc*$^-$ strain in general produces much less pigments than the wild type, in particular under microaerobic conditions. Since the pigments are required to build the photosynthetic complexes, lower pigment production will result in decreased amounts of pigment–protein complexes.

2.2 | RNA-seq analysis reveals global effects of RNase III on gene expression in *R. sphaeroides*

We previously showed that RNase E has a remarkably strong effect on the growth of *R. sphaeroides* under phototrophic conditions

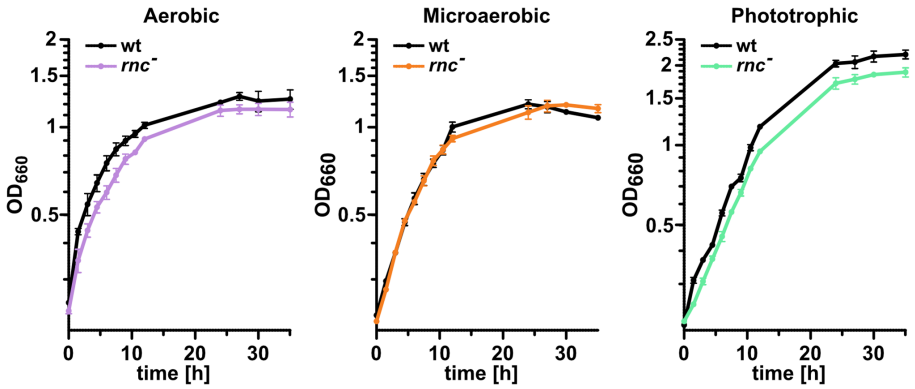

FIGURE 1 Growth behaviour of the *rnc*$^-$-mutant strain under various growth conditions. The growth behaviour of the *R. sphaeroides* wild type and *rnc*$^-$ strain was analysed by monitoring the optical density (OD_{660}) over 35 h. Cells were either cultivated under aerobic, microaerobic or phototrophic conditions in a malate minimal medium. The mean value of biological triplicates is shown. The standard deviation is given as error bars.

that correlate with strong changes of the transcriptome (Börner et al., 2023; Förstner et al., 2018). We were also interested in investigating the global effects of RNase III on the transcriptome especially in regards to growth under different environmental conditions. We cultivated the *rnc*⁻ mutant and wild type under aerobic, microaerobic or phototrophic conditions to mid-exponential growth phase and collected samples for RNA-seq analysis. To compare the RNA expression profiles, we performed unsupervised agglomerative hierarchical clustering, grouping all transcripts according to their expression level between two growth conditions, in either wild type or mutant (Figure 3).

To first investigate the growth condition-dependent effect on RNA abundance changes, all transcripts with $\log_2$ fold change >1 or <−1, adjusted *p*-value <0.05 (between two growth conditions) and a minimum of at least 10 reads in one library were counted as significantly differentially regulated between two growth conditions. For further analysis of the RNase III-dependent influence on the transcriptome, the RNA expression profiles of all significantly differentially regulated genes (from the comparison of the two growth conditions) within wild type or mutant were plotted side by side in the form of three independent heat maps (Figure 3). While the majority of the transcriptome showed very similar expression changes between mutant and wild type (visible in a similar blue/red tone between wild type and mutant column), some RNAs showed different expression changes between the two strains (selected regions of interest are marked as 1–9 in Figure 3). The number of RNAs contained per each region and their annotated features are shown in Table 1. A list of all RNAs per region is shown in Supplementary Table S1.

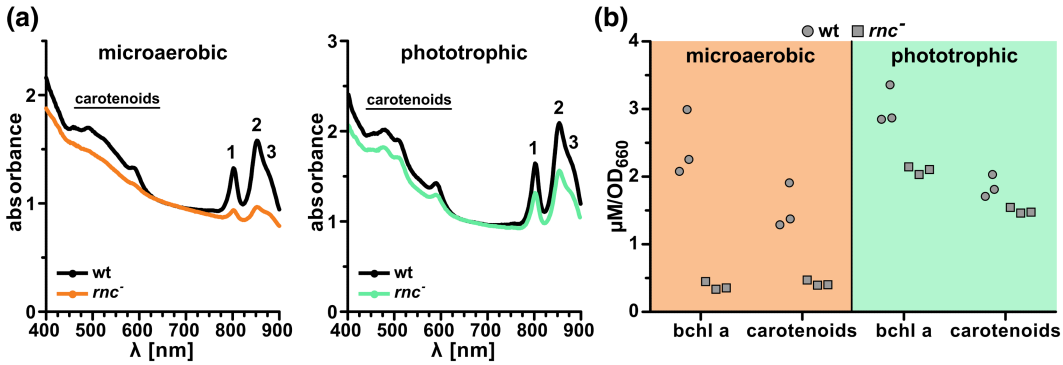

FIGURE 2 Loss of RNase III activity leads to impaired production of photosynthetic complexes. (a) Whole-cell absorbance spectra of microaerobically or phototrophically grown wild type and mutant cells. The specific absorbance maxima for photosynthetic complexes are marked as 1–3 (1: RC and LH II; 2: LH II; 3: RC and LH I). The mean values of biological triplicates are shown. (b) Photometrically determined amounts of bacteriochlorophyll a (bchl a) and carotenoids from acetone/methanol extracts of wild type and mutant cells. The strains were grown under phototrophic or microaerobic conditions as biological triplicates.

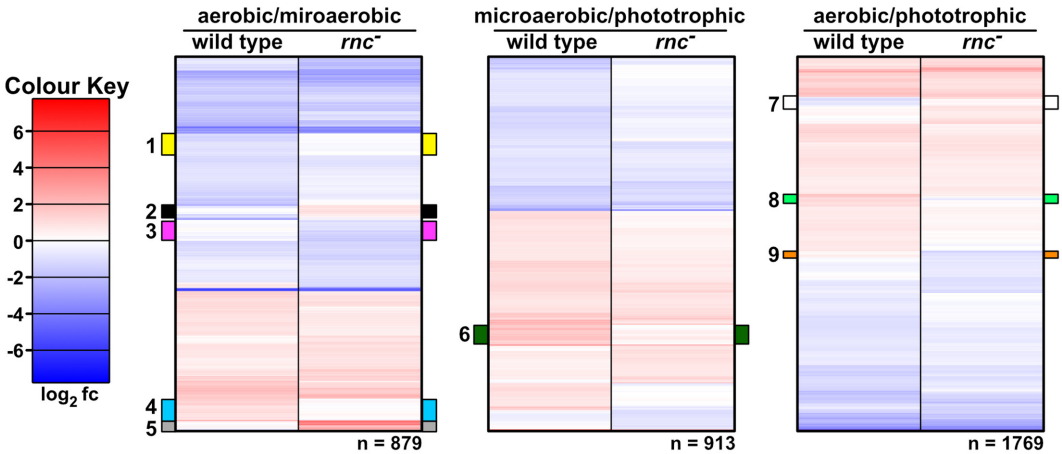

FIGURE 3 RNA-seq-based global RNA expression patterns. Heat maps illustrate global changes in RNA expression between the different growth conditions, within wild type or mutant. Ratios ($\log_2$ fold changes) were calculated from RNA-seq data obtained from aerobically, microaerobically or phototrophically grown biological triplicates of wild type (left panel) or *rnc*⁻ (right panel) strain. All RNAs with significantly differential abundances ($\log_2$ fold change >1 or <−1, p-adjusted value <0.05, with a mean read count of at least 10 between all samples) were plotted per heat map. RNAs within one heat map were grouped into clusters according to their expression pattern between the two indicated growth conditions within a strain by unsupervised agglomerative hierarchical clustering. The total number of displayed RNAs is indicated at the bottom right of each heat map. A positive expression change is highlighted in red and a negative expression change in blue colour (colour key).

TABLE 1 Distribution of functional RNA types among regions of the heat maps.

Region	RNAs in total	rRNA	tRNA	sRNA	mRNAs with predicted function	mRNAs for hypothetical proteins
1	47	2	–	–	20	15
2	27	–	1	3	12 (5)	11 (3)
3	40	–	–	–	13	27
4	47	–	6	–	22	19
5	23	–	–	2	7	14
6	46	–	–	–	29	17
7	44	3	5	1	13 (7)	21 (5)
8	13	–	–	–	8	5
9	11	–	–	–	5	6

Note: The table shows the total content of RNAs per region of the heat maps from Figure 3. The number of contained RNAs was further divided according to their annotated RNA type (rRNA, tRNA, sRNA and mRNA). The numbers per annotated type are given in the following rows. mRNAs with predicted function and mRNAs for hypothetical proteins are separately listed. Numbers in parentheses indicate the amount of RNAs located in close proximity downstream to one of the rRNA operons.

For most of the defined regions, no functional groups among the genes are obvious. Region 1 contains the *traB*, *F*, *G*, *N* and *W* genes for proteins related to plasmid conjugation and *groEL* and *groES* for heat shock chaperonins. As well, *tra* genes as *gro* genes are co-transcribed. While *groEL* and *groES* are localised on chromosome I, *tra* genes are localised on mega plasmid D. Region 6 contains several genes involved in metal transport (*znuAB*, *zur* and *sitD*).

Interestingly, when looking at the read coverage files using the Integrated Genome Browser (Freese et al., 2016), we noticed that a large proportion of enriched RNAs in the mutant are located directly downstream of rRNA operons (one rRNA operon is located on the large first chromosome, and two more rRNA operons on the second chromosome) (Figure 4). A screenshot visualising the total RNA-seq read coverage at the genomic locus of the first rRNA operon, taken from the Integrated Genome Browser, is shown in Figure S3. A list of all genes located directly downstream to rRNA operons (as seen in Figure 4), including the DESeq2 results (mutant/wt under microaerobic conditions) of those genes, is given in Supplementary Table S2. To validate the enrichment of RNAs located directly downstream of the rRNA operons, as seen in the RNA-seq read coverage (Figure 4), qRT-PCR was performed for four different loci, located downstream of the rRNA operons (locus A and locus B: downstream to rRNA operon 1; locus C: downstream to rRNA operon 2; locus D: downstream to rRNA operon 3). qRT-PCR for all four tested loci confirmed high enrichment of the tested RNA segments in the *rnc*$^-$-mutant strain compared to the wild type under microaerobic conditions (Figure 4c), as also seen in the read coverage plots in Figure 4a,b as well as the DESeq2 results shown in Supplementary Table S2. To test, if the enrichment of these loci is due to increased transcription, possibly by partially unterminated transcription read-through of the rRNA genes, we chromosomally integrated additional transcription terminators directly downstream, adjacent to the rRNA operons in the *rnc*$^-$-mutant strain by homologues recombination (insertion regions are marked as green arrows in Figure 4a,b), and repeated qRT-PCR for the four different loci A-D with samples of the modified *rnc*$^-$ mutants, harbouring additional transcription terminators. Strikingly, we observed a strong reduction of RNA abundances, compared to the quantification of the previous *rnc*$^-$ samples with native transcription terminators. While still being slightly enriched, the RNA abundances at all four loci nearly reached wild type level.

To further characterise the effects of RNase III on the *R. sphaeroides* transcriptome, we used an RNA-seq-based prediction protocol to globally map bona-fide RNase III cleavage sites, comparable to approaches recently published by our group for RNase E (Börner et al., 2023; Förstner et al., 2018). For this, we analysed the 5′ end positions of each RNA-seq read obtained from wild type and *rnc*$^-$ strain under aerobic, microaerobic or phototrophic growth conditions. As an endoribonuclease, RNase III can cleave RNA substrates internally and as a result may generate new stable RNA 5′ ends. If stable, these new 5′ ends will consequently produce higher 5′ end read counts at positions, where RNase III catalysed RNA hydrolysis (RNase III-dependent 5′ ends). As a consequence, these RNase III-dependent 5′ end read counts can be enriched in the wild type, in comparison to the mutant (where RNase III is unable to hydrolyse RNAs), and were further defined by us as significantly enriched in the wild type with setting cut-off parameters as $\log_2$ fold change >1 (wt/mutant) and adjusted *p*-value <0.05, with a minimum read count of at least 10 in one of the libraries (from now on referred to as RNase III cleavage sites).

Through our prediction approach, we were able to identify RNase III cleavage sites under all three tested growth conditions, where most sites were detected under aerobic conditions ($n = 2220$), less under phototrophic conditions ($n = 1093$) and least under microaerobic conditions ($n = 565$) (Figure 5a). The biggest overlap of cleavage sites was found between microaerobic/phototrophic and microaerobic/aerobic conditions, which reflects that microaerobic conditions represent an intermediate state between growth at high oxygen conditions (aerobic) and complete absence of oxygen (phototrophic).

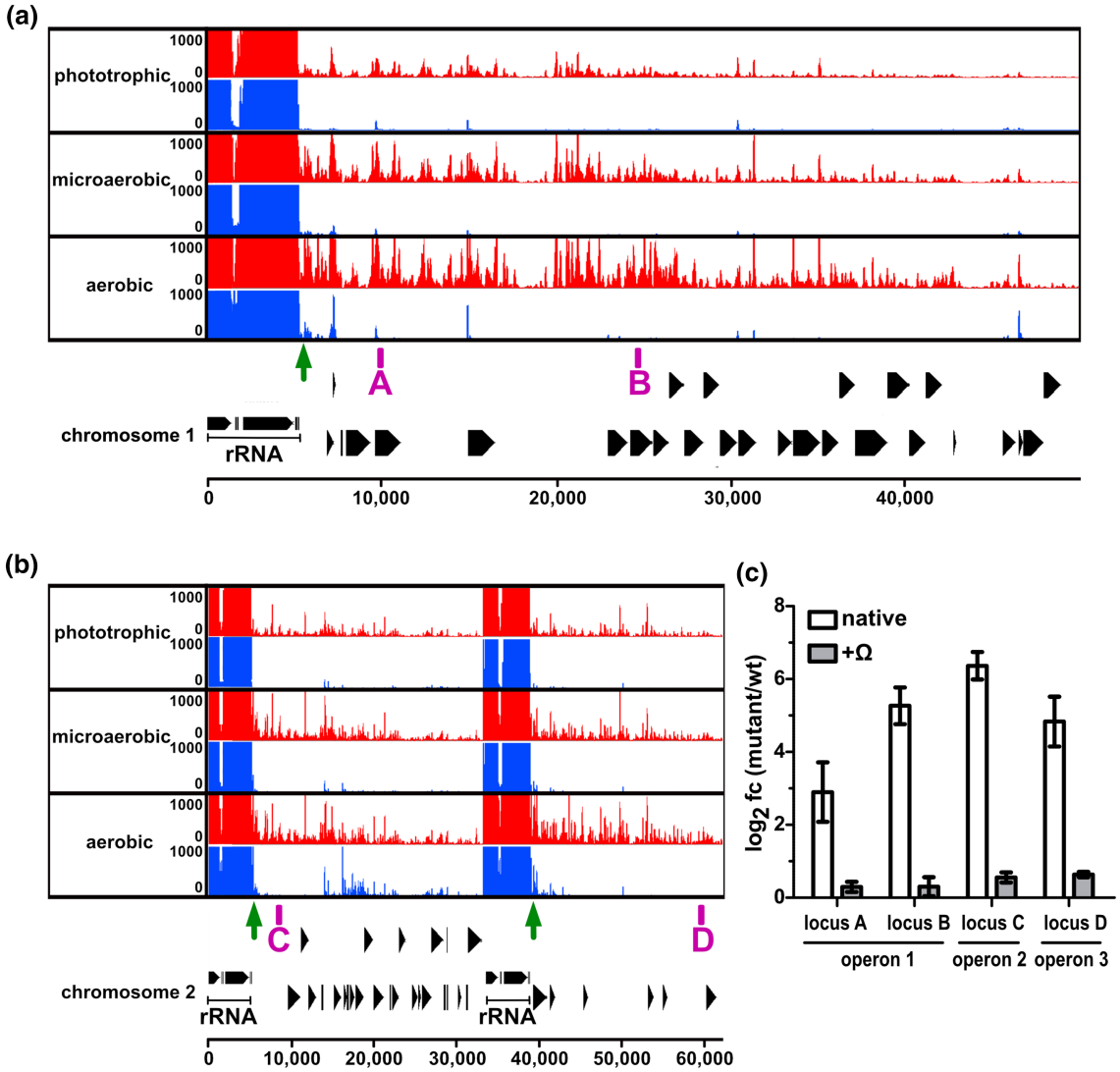

FIGURE 4 RNA-seq read coverage of the genomic regions located downstream to rRNA operons. (a,b) The total read coverage of cDNA libraries from exponentially grown wild type (blue) and *rnc*⁻ (red) strain samples is shown. Samples were collected during growth under either aerobic, microaerobic or phototrophic conditions. The read coverage was plotted from wiggle files of merged independent biological triplicates with the integrated genome browser. The scale bar of the read coverage has an identical height for all tracks. Annotated genes are shown in black. Green arrows indicate the locations, where transcriptional terminators have been chromosomally integrated. Validation by qRT-PCR was performed for four different loci (A–D; magenta boxes). (c) Spike-in qRT-PCR for quantification of RNA loci located downstream of the three rRNA operons. 20 ng DNA-free total RNA of microaerobically grown biological triplicates of *R. sphaeroides* wild type and *rnc*⁻ strain were analysed (white bars). Additionally, wild type samples were compared to modified *rnc*⁻ strains, harbouring inserted transcriptional terminators directly downstream of the rRNA operons (see panels a and b of this figure). The relative abundance (mutant/wt) is shown. The standard deviation of the mean is indicated as an error bar.

To characterise the cleavage sites on a global scale, we grouped the RNAs harbouring cleavage sites among annotated genomic features (Figure 5b). Our analysis revealed a predominant quantity of cleavage sites within coding sequences (CDS), where most cleavage sites were found under aerobic conditions, followed by phototrophic conditions, and least under microaerobic conditions. The second biggest group to contain RNase III cleavage sites were ribosomal RNAs, followed by 5′ UTRs and sRNAs.

Additionally, we quantified the cleavage site per RNA ratios under each of the three growth conditions and found an enormous variation of cleavage sites per RNA (Figure 5c). The vast majority of RNAs lacked any RNase III cleavage site (≈85% under aerobic conditions; ≈95% under microaerobic conditions; ≈89% under phototrophic conditions), while second most RNAs contained a single RNase III cleavage site. Interestingly, we could identify several RNAs with more than 50 cleavage sites per transcript, nearly exclusively under phototrophic conditions. The highest number of sites per RNA was found within all three copies of 23S rRNA under phototrophic conditions (each with 75 sites per RNA), followed by 16S rRNA (66, 51 and 47 sites RNA). Under aerobic conditions, the *fusA1* transcript, encoding translation elongation factor G, was detected as the RNA with the most cleavage sites (57 sites).

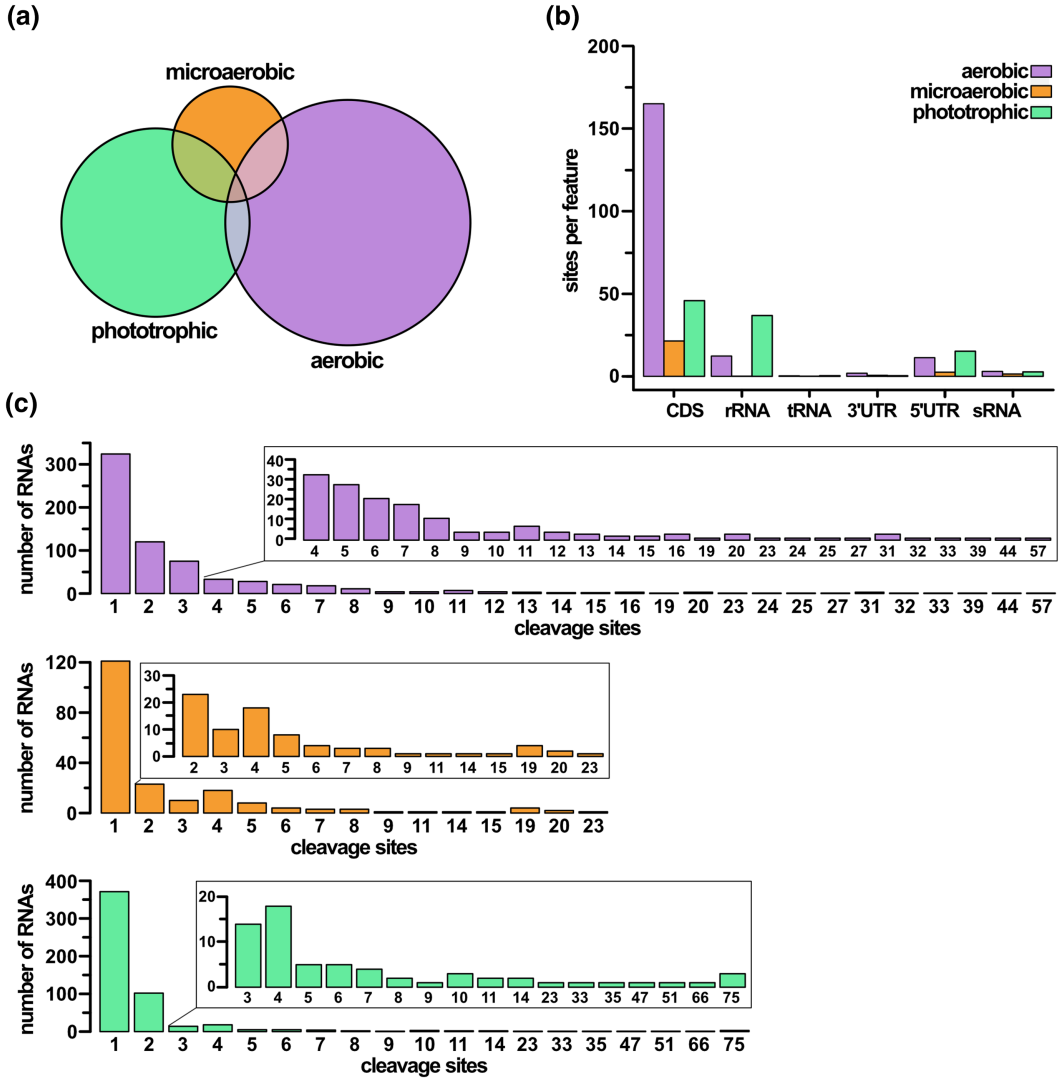

FIGURE 5 Distribution of mapped RNase III cleavage sites. (a) Amount of mapped RNase III cleavage sites per growth condition. The circle and overlaps illustrate the proportional quantity of identified RNase III cleavage sites. (b) Distribution of cleavage sites per annotated genomic feature. (c) Number of RNAs and their respective amount of identified cleavage sites.

Since our analysis pointed towards high amounts of RNase III cleavage sites especially under aerobic conditions, we constructed an in vivo RNase III activity reporter (equivalent to our recently published ribonuclease E activity reporter, Börner et al., 2023) to study the growth condition-dependent effects of RNase III. We fused the well-characterised RNase III cleavage site of the native pre-16S rRNA to the mVenus encoding gene (indicator construct: pPHU231-5′UTR-mV), allowing RNase III to introduce cleavage within the 5′ UTR of the reporter mRNA generating a monophosphorylated 5′ end, which can subsequently activate 5′ end-dependent RNA decay by RNase E. As a background control for RNase III activity on mVenus expression, we used an almost identical plasmid, with the sole exception, that it did not contain the introduced cleavage site but only the ribosome binding site within the 5′ UTR of mVenus (control construct: pPHU231-p16S-mV). The scheme of both reporter constructs is depicted in Figure 6a.

After conjugation of the reporter plasmids to either wild type or *rnc*⁻ cells, we cultivated the resulting conjugants under aerobic, microaerobic or phototrophic conditions and determined the normalised fluorescence units (F/OD_{660}) of the mid-exponential cultures in a Tecan plate reader. A strong effect of the growth conditions on the measured fluorescence was visible, which is partly due to the influence of oxygen on mVenus fluorescence. Only a minor difference in normalised fluorescence units was observed between wild type and *rnc*⁻ cells for the control construct, as the wild type produced only slightly higher fluorescence values (Figure 6b). On the other hand, a strong effect of the RNase III deficiency in the form of highly elevated fluorescence units generated by the indicator construct was visible (Figure 6c), which served as a proof of function of our construct. Interestingly, we did not observe an equal ratio in fluorescence of wild type to mutant throughout the three growth conditions: the fluorescence units under microaerobic and phototrophic conditions differed by factors of 1.9 and 2.6, respectively,

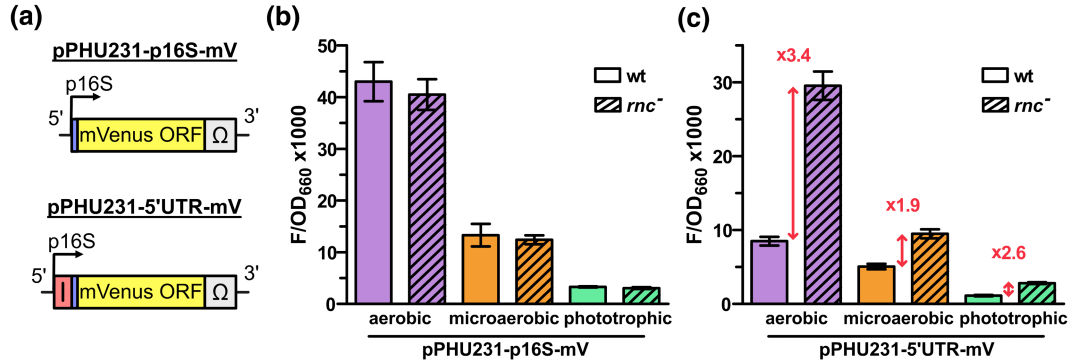

FIGURE 6 Reporter system-based evaluation of the in vivo RNase III cleavage activity. (a) Schematic overview of the reporter constructs. The mVenus gene (yellow) is under transcriptional control of the strong constitutive 16S rRNA promoter of *R. sphaeroides*, preceded by an optimised artificial ribosome binding site (blue), and followed by a transcriptional terminator (grey) (control construct: pPHU231-p16S-mV) as described in Börner et al. (2023). To investigate RNase III cleavage activity, the well-characterised RNase III cleavage site of the native 5′ pre-16S rRNA (red) was introduced in the 5′ UTR directly upstream of the ribosome binding site (indicator construct: pPHU231-5′UTR-mV). Biological triplicates of wild type and *rnc*⁻ mutant, carrying the reporter plasmids pPHU231-p16S-mVenus (b) and pPHU231-5′UTR-mVenus (c) were cultivated under aerobic, microaerobic or phototrophic conditions until exponential growth phase. The mean values of normalised fluorescence intensities (F/OD_{660}) and their standard deviations are shown. The ratio between wild type and mutant mean values is indicated in red colour above the two corresponding bars.

while under aerobic conditions, a stronger increment (factor 3.4) was measured. This supports variations of the impact of RNase III under different growth conditions.

2.3 | Elevated CcsR expression is accompanied by increased resistance towards oxidative stress upon loss of RNase III activity

Recent studies of our group identified a novel small RNA-binding protein, CcaF1, which is co-expressed with four homologous CcsR sRNAs (CcsR1-4) from a single promoter (Billenkamp et al., 2015; Grützner, Billenkamp, et al., 2021). While CcaF1 binds to various RNA targets (Grützner, et al., 2023; Grützner, Billenkamp, et al., 2021), affecting their stability and regulating gene expression, the CcsR sRNAs inhibit a glutathione-dependent C1 metabolic pathway, leading to increased levels of antioxidative glutathione, which provides protection against reactive oxygen species and enhancing cell viability. Previous work documented a direct correlation between CcsR levels and stress resistance (Billenkamp et al., 2015; Grützner, Billenkamp, et al., 2021).

As our RNA-seq data indicated a strong enrichment of CcsR sRNAs in the *rnc*⁻ mutant compared to the wild type in the presence of oxygen (read coverage shown in Figure S4a,b), we were interested in further validating these results. To investigate the expression of CcsR, especially in regard to its function during stress conditions, we induced the stress response of *R. sphaeroides* through incubation at an elevated temperature (42°C) or treatment with paraquat (superoxide radical-inducing agent), $CdCl_2$, H_2O_2 or tBOOH (tertiary butyl alcohol, organic hydroperoxide), followed by isolation of total RNA. Northern blot analysis confirmed the RNA-seq result of an enriched CcsR1 steady-state level in the mutant during standard microaerobic growth conditions at 32°C (Figure 7a). The sequence of the four CcsR sRNAs is almost identical, but the chosen oligonucleotide probe allows specific detection of CcsR1, which is representative of CcsR1-4 levels (Billenkamp et al., 2015). For all tested stress conditions, both strains showed an increase in CcsR1 expression, which confirms the induction of stress condition, as CcsR is transcribed from an RpoHI/RpoHII-dependent promoter. RpoHI and RpoHII are alternative sigma factors, actively replacing the house-keeping sigma factor during heat and oxidative stress in *R. sphaeroides* (Nuss et al., 2010). Interestingly, the mutant showed much higher CcsR1 levels than the wild type under all tested stress conditions, except for heat stress, where CcsR1 expression was slightly reduced in the mutant compared to the wild type. Furthermore, we analysed CcsR1 expression by northern blot analysis of total RNA samples from the *rnc* complementation strain (*rnc*⁻::pRK-*rnc*). Restoration of the wild type-like CcsR1 abundance within the complementation strain proved the influence of RNase III on CcsR1 expression (Figure 7b).

As the RNA steady-state level is defined by the individual transcription rate, as well as the RNA stability, we constructed a reporter plasmid harbouring a transcriptional fusion of the CcsR expression controlling pCcaF1 promoter and the gene of the yellow fluorescent protein mVenus (pPHU-pCcaF1-mV). The reporter plasmid and the related empty control vector were transferred to *R. sphaeroides* wild type and *rnc*⁻ cells by diparental conjugation. Fluorescence measurements of the microaerobically grown conjugants revealed a stronger reporter signal within the *rnc*⁻ background (fluorescence units around 35% increased), pointing towards higher promoter activity and more frequent transcription of CcsR from pCcaF1 upon loss of RNase III activity (Figure 7c).

As the CcsR sRNAs are transcribed from an RpoHI/RpoHII-dependent promoter, we also quantified mRNA level for the alternative sigma factors RpoE, RpoHI and RpoHII by qRT-PCR (Figure S5). The results show that *rpoE* and *rpoHII* mRNA levels were increased in the *rnc*⁻ mutant compared to the wild type. As a master regulator,

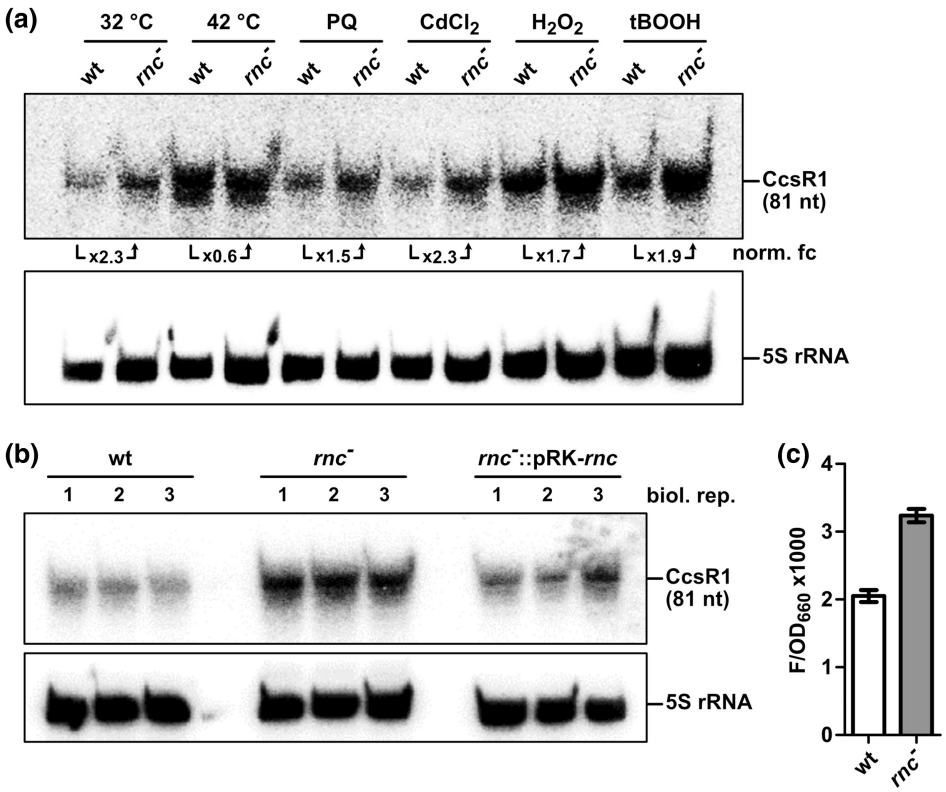

FIGURE 7 RNase III affects stress-dependent expression of CcsR. Northern blot analysis for evaluation of the CcsR1 sRNA steady-state level. 7 µg total RNA from microaerobic cells were analysed. RNAs were detected by hybridisation with a radiolabelled antisense DNA probe specific for CcsR1. Visualisation of the 5S rRNA served as a loading control. (a) To induce the stress response, wild type and *rnc*⁻ cultures were either grown for 1 h at 42°C or treated with 0.3 mM paraquat (PQ), 0.1 mM $CdCl_2$, 0.5 mM H_2O_2 or 0.3 mM tBOOH prior to sample collection and RNA isolation. The fold change (mutant/wt) after normalisation to the loading control is indicated below the corresponding bands. (b) RNA originating from biological triplicates of wild type, *rnc*⁻ mutant, and the RNase complementation strain (*rnc*⁻::pRK-*rnc*) was analysed by northern blot. (c) In vivo promoter activity reporter assay. Microaerobically grown biological triplicates of wild type and mutant cells, carrying the transcriptional fusion of pCcaF1 and mVenus on plasmid pPHU-pCcaF1-mV, were used for measurements of mVenus fluorescence intensity. Mean values of the normalised fluorescence units (F/OD_{660}) and their standard deviations are shown.

RpoE activates the expression of RpoHII in *R. sphaeroides*, specifically during oxidative and heat stress conditions (Dufour et al., 2012; Nuss et al., 2009). Interestingly, with our RNA-seq-based prediction approach, no bona fide RNase III cleavage sites were mapped to either of the mRNAs.

To investigate the transcript stability of CcsR in vivo, we cultivated the wild type and *rnc*⁻ strain under microaerobic conditions to mid-exponential growth phase (≈OD_{660} 0.5) and added rifampicin to inactivate the DNA-dependent RNA polymerase. Samples collected either prior to the addition of rifampicin (referred to as 100% RNA content), or after rifampicin addition were used for northern blot analyses. The half-life experiments confirmed our previously obtained data of a generally enriched CcsR1 steady level in the *rnc*⁻ strain. Interestingly, we did not observe a major difference in transcript stabilities, between mutant and wild type strain, as the northern blot signal for the mutant samples only decreased slightly faster than the signals from the wild type samples (Figure 8a). To calculate the half-lives of CcsR1 in the different strains, we quantified the CcsR1 signals and normalised them to the signal intensities of the 5S rRNA loading control, followed by fitting the normalised data points to semi-logarithmic trend lines. The calculation revealed only a minor difference in CcsR1 stability, with a calculated half-life of around 7.1 min for the wild type and around 6.4 min for the mutant (Figure 8b).

Since the mutant strain accumulates CcsR through increased transcription rate, and one function of CcsR is to downregulate glutathione-dependent metabolism in *R. sphaeroides* helping to counteract oxidative stress, we next tested the survival of the mutant strain under certain stress conditions. For this, we selected several stress agents causing oxidative cell damage, and treated exponentially grown wild type and mutant cells. To assess stress resistance and subsequent cell survival rate, we plated a dilution of the treated cultures on agar plates and counted resulting colonies from the differentially treated approaches after 2 days of growth at 32°C in the dark. An untreated approach, where no stress-inducing agents were added, served as a reference (100% cell survival rate) (Figure 9a). Our data show comparable survival rates of mutant and wild type strains after exposure to elevated temperatures at 42°C (heat shock, causing protein denaturation) or treatment with cadmium chloride. As a heavy metal, cadmium acts toxic on cells, causing protein denaturation through disruption of protein disulphide bridges, and release of protein-bound Fe^{2+} through binding

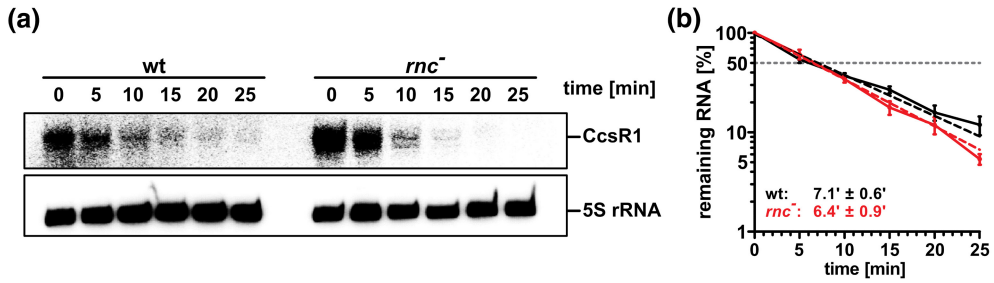

FIGURE 8 The stability of CcsR is unaffected by a loss of RNase III activity. (a) Northern blot analysis for evaluation of the CcsR1 half-lives. Microaerobic wild type and *rnc*⁻-mutant cultures were treated with 0.2 mg/mL rifampicin. Samples were collected prior ($t = 0$ min) and 5, 10, 15, 20 and 25 min after the rifampicin treatment. 10 µg total RNA were electrophoretically separated on a denaturing 10% polyacrylamide gel and subsequently immobilised on a nylon membrane by blotting and UV crosslinking. RNAs were detected by hybridisation of the membrane with a radiolabelled antisense DNA probe specific for CcsR1. Visualisation of the 5S rRNA served as a loading control. (b) Decrease of CcsR1 sRNA levels after rifampicin treatment. Transcript stabilities were calculated by quantification of the northern blot signal intensities of wild type (black) and mutant (red) samples, normalisation to the loading control and fitting of the data points to semi-logarithmic trend lines (dashed lines). Northern blots with samples from independent biological triplicates of wild type and mutant were used for calculation.

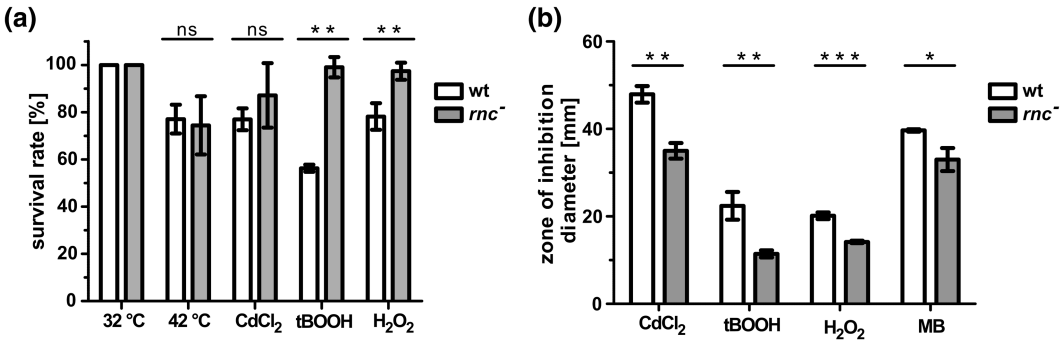

FIGURE 9 RNase III affects the stress resistance of *R. sphaeroides*. (a) Normalised survival rates (cfu/mL) of wild type and mutant under several stress conditions. The mean values and their standard deviation of normalised biological triplicates are shown as white (wild type) and grey (mutant) bars. Cells grown at 32°C served as a reference. For assessing survival, the cultures were shifted to 42°C for 1 h (heat shock) or incubated with either 0.01 mM $CdCl_2$, 0.3 mM tBOOH or 0.5 mM H_2O_2 for 20 min before plating on solid malate minimal medium. Student's two-sided t-test was used to assess the statistical significance of the difference in mean values (ns: not significant; ***p*-value <0.01). (b) Zone of inhibition assay showing the stress resistance of wild type (white) and mutant (grey) cells on a solid medium. 0.1 M $CdCl_2$, 0.5 M tBOOH, 1 M H_2O_2 or 0.01 M methylene blue (MB) were spotted on sterilised filter discs in the centre of *Rhodobacter*-containing soft agar plates. The mean zone of inhibition diameter of biological triplicates is depicted. Standard deviations are given as error bars. Student's two-sided *t*-test was used to assess the statistical significance of the difference in mean values (**p*-value <0.05, ***p*-value <0.01, ****p*-value <0.001).

competition with divalent cation co-factors leading to the generation of hydroxyl radicals by the Fenton reaction and other reactive oxygen species by downstream processes. For cultures treated with tBOOH (organic peroxide) or H_2O_2, we observed a higher rate of colony-forming units from the mutant compared to the wild type, comparable to the colony-forming units of the untreated approach, indicating an increased stress resistance under these conditions.

In addition to our stress experiments with liquid cultures, we performed zone of inhibition assays to evaluate the stress resistance of both strains grown on a solid medium (Figure 9b). Notable, a more pronounced zone of inhibition in this assay indicates a decreased stress resistance. Interestingly, the mutant strain showed significantly smaller zones of inhibition than the wild type after treatment with cadmium chloride, which suggests an elevated stress resistance of the mutant against cadmium toxicity on a solid medium, and is more pronounced than the respective stress resistance in liquid medium (Figure 9a). For tBOOH and H_2O_2 stress, the zone of inhibition data showed similar results as previously obtained from the survival assay (indicating a higher stress resistance of the mutant). Additionally, we tested the photooxidative stress resistance of the mutant by applying methylene blue onto the culture containing soft agar plates, followed by incubation under white light. In this approach, methylene blue acts as a photosensitiser by energy transfer to molecular triplet oxygen and subsequent electron spin-flip leading to the generation of singlet oxygen, in the presence of light (DeRosa & Crutchley, 2002). As already observed for cultures treated with $CdCl_2$ or peroxide, the mutant strain showed a higher survival rate than the wild type.

In addition to small regulatory RNAs, ROS-detoxifying enzymes like superoxide dismutases and catalases play a well-studied and crucial role in counteracting oxidative stress. While the model organism *E. coli* possesses three superoxide dismutase enzymes (*sodA*, *sodB* and *sodC*), only a single superoxide dismutase has been found in *Rhodobacter capsulatus* (Cortez et al., 1998) and a single superoxide dismutase (*sodC*) is annotated in *R. sphaeroides*. Nevertheless, our RNA-seq approach did not reveal any effect of RNase III on the abundance of *sodC* in *R. sphaeroides*. Interestingly, the catalase encoding mRNA, *catA*, showed an increased steady-state level in the *rnc*⁻ mutant in our RNA-seq data, which also was validated by qRT-PCR with a $\log_2$ fold change ≈ 1.8 (mutant/wt) under microaerobic growth conditions. *catC*, which encodes another catalase in *R. sphaeroides* showed no expression changes between wild type and RNase III mutant in our RNA-seq analysis under all three growth conditions (data not shown).

Taken together, our data indicate a higher stress resistance of the mutant against all tested ROS-causing agents, except for $CdCl_2$ on solid media (while here also a higher mean cfu/mL was calculated, the standard deviation between the independent biological replicates was too large to be considered as significant). A higher stress resistance upon heat shock could not be seen in our data.

2.4 | RNase III controls quorum sensing in *R. sphaeroides*

Since its first discovery in *Aliivibrio fischeri* (Nealson et al., 1970), quorum sensing (QS) has been intensely investigated in many bacterial species and has been described as the ability to sense and respond to cell density in a bacterial population. The well-studied LuxI/LuxR QS system of *A. fischeri* comprises besides five other proteins a signal receptor (LuxR) sensing the presence of autoinducer molecules and controlling the transcription of QS-regulated genes, and an autoinducer synthase (LuxI), whose expression is induced upon perceived QS signals (Engebrecht & Silverman, 1984). The existence of Lux-type systems has later been reported for many bacterial species (Fuqua et al., 1994; Greenberg et al., 1979; Salmond et al., 1995), underlining its biological relevance. While the LuxI/LuxR-type system is one of the most simply built, a variety of more complex QS systems has been described in last decades, where a surprisingly high amount of physiological functions have been found to show QS-dependent regulation (e.g. antibiotic production/resistance, virulence, biofilm formation, sporulation or morphology) (reviewed in Miller & Bassler, 2001; Whitehead et al., 2001).

In *R. sphaeroides*, the LuxR-type signal receptor is encoded by the *cerR* gene, whereas *cerI* codes for the LuxI-type acyl-homoserine lactone (AHL, autoinducer) synthase. RNA-seq data of the *rnc*⁻-mutant strain revealed an elevated *cerI* mRNA level under microaerobic and phototrophic conditions, where the enrichment over the wild type was highest under microaerobic conditions (Figure S6). To test whether the accumulation of *cerI* mRNA in *R. sphaeroides* has any physiological effect on AHL production, we used an *S. meliloti* reporter strain (McIntosh et al., 2019). This strain is characterised by a disrupted QS system unable to synthesise AHLs. Additionally, the strain carries a low copy reporter plasmid, introducing a transcriptional fusion of promoter pSMb20911 with the mVenus gene. In this in vivo system, pSMb20911 is repressed by rising AHL concentrations and thereby the expression of mVenus is negatively regulated. This coupling between rising AHL concentration and decreasing fluorescence signal enables to quantify unknown AHL concentrations.

To assess the correlation between fluorescence signal and AHL concentration, we collected cell-free supernatant from mid-exponential *R. sphaeroides* wild type cultures and incubated separate reporter strain cultures with increasing ratios of supernatant per blank medium (growth in 0%–100% supernatant). The resulting fluorescence units were plotted and used as reference correlation (Figure 10a, grey box). To quantify the AHL amounts produced by the *rnc*⁻ strain, we next compared fluorescence units of the in vivo system, generated through incubation with 25% cell-free supernatant from mutant or wild type. Remarkably, a strongly diminished signal (≈1500 F/OD_{600}) was obtained from reporter cultures grown with supernatant of the *rnc*⁻ strain, which was even lower than the signal generated by growth in 100% wild type supernatant (≈2200 F/OD_{600}), indicating immense repression of mVenus caused by hyperproduction of AHLs in the *rnc*⁻ mutant (factor: >4). As a control, we tested the effect of 400 nM commercially obtained AHL on our reporter system, which resulted in just slightly fewer fluorescence units (≈1000 F/OD_{600}) than measured while evaluating the *rnc*⁻ strain supernatant (Figure 10a).

To validate the effects on the *cerI*/*cerR* system observed in our RNA-seq data (Figure S6), we analysed the total RNA of independent biological triplicates from wild type and *rnc*⁻ strain by qRT-PCR (Figure 10b). As expected, the mutant showed a strong enrichment of *cerI* transcript compared to the wild type ($\log_2$ fold change mutant/wt ≈ 2.5), while for *cerR* only a mild effect was visible. Since the LuxI/LuxR-type system represents a positive feed-forward loop, the accumulation of autoinducer leads to an increment of the *cerI* mRNA level, through decreased repression of *cerI* transcription by *cerR*. Nevertheless, we were interested to further investigate the impact of RNase III on this system by analysis of the in vivo *cerI* mRNA stabilities in the wild type and *rnc*⁻ background. For this, we added rifampicin to exponentially grown wild type and mutant cultures, collected samples at distinct time points after addition of rifampicin and analysed the total RNA of these samples by qRT-PCR. As a result, we plotted the decreasing *cerI* mRNA level per time and fitted the data points to semi-logarithmic trend lines. While the wild type showed a specific *cerI* half-life of around 4 min, our analysis revealed an increased stability in the mutant with a half-life of around seven to 9 min, indicating a relevant destabilising effect on RNase III on the *cerI* transcript.

3 | DISCUSSION

Our comparative RNA-seq analysis revealed a considerable impact of RNase III on the transcriptome of *R. sphaeroides* that was,

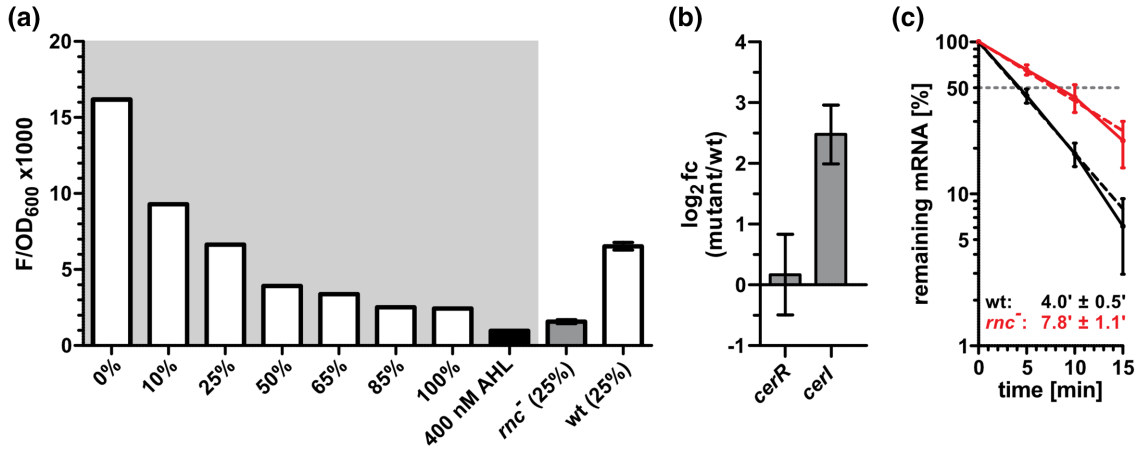

FIGURE 10 The production of quorum-sensing autoinducer molecules is negatively affected by RNase III. (a) In vivo reporter system for detection of quorum-sensing autoinducer levels. An *S. meliloti* reporter strain (McIntosh et al., 2019) was used to evaluate concentrations of secreted autoinducer molecules from cell-free supernatants of wild type (white) and *rnc*⁻ (grey) cultures. The *S. meliloti* reporter strain was grown in increasing amounts (0%–100%) of supernatant from microaerobically grown *R. sphaeroides* wild type cultures (assessment of repression, grey box) or in 25% supernatant from the microaerobically grown *R. sphaeroides rnc*⁻ strain. A reporter culture grown with 400 nM oxo-C16:1-HL served as a reference (black bar). The resulting mVenus expression is shown as normalised fluorescence (F/OD_{600}). (b) Spike-in quantitative reverse transcriptase PCR for quantification of *cerR* and *cerI* from *R. sphaeroides* wild type and *rnc*⁻ strain. 20 ng DNA-free total RNA of microaerobically grown biological triplicates was analysed. The relative abundance (mutant/wt) is shown. The standard deviation of the mean is indicated as an error bar. (c) Determination of *cerI* transcript stabilities in wild type and mutant strain. 20 ng DNA-free total RNA, isolated from cell samples collected either prior ($t = 0$ min) or 5 min, 10 min, 15 min after the addition of 0.2 mg/mL rifampicin, were analysed by spike-in quantitative reverse transcriptase PCR. Mean values of biological triplicates were fitted to semi-logarithmic trend lines (dashed lines).

however, less pronounced than the impact of RNase E (Börner et al., 2023). An unexpectedly high amount of enriched RNAs in the mutant originated from loci directly downstream of rRNA operons (Figure 4), resulting in a strongly increased read coverage obtained by RNA-seq that was confirmed for selected genes by qRT-PCR. We hypothesised that these increased transcript levels are due to partially unterminated transcription of the rRNA genes leading to read-through into the downstream located genes, or due to increased DNA accessibility, for example, by a higher degree of DNA structure relaxation in the mutant strain. The chromosomal insertion of additional transcription terminators directly downstream to rRNA operons resulted in a drastic decrease of the tested transcript levels (Figure 4c), nearly restoring wild type-like RNA abundances, suggesting that transcription termination of rRNA is affected in the *rnc*⁻ strain. In a recently published RNA-seq study with an *E. coli* RNase III mutant (Maes et al., 2017), such an enrichment of transcripts located downstream to rRNA was not visible. As for our own data set, no rRNA depletion was applied to the chosen *E. coli* data set. This implies an effect of RNase III that is not general but maybe specific to bacteria with RNase III-dependent 23S rRNA fragmentation. Presently, this possibility cannot be validated due to the lack of suitable data sets.

The biosynthesis of rRNA, including transcription elongation and rRNA processing, is a highly complex but crucial growth-rate limiting step, which is only poorly understood in many bacterial species. The elongation of rRNA transcription has been reported to include several factors, importantly, the Nus proteins involved in anti-termination at several rho-dependent termination sites. To achieve anti-termination and to promote read-through, NusA and NusB can assemble with RNA sequences of the nascent rRNA transcript, known as *boxA* sites, and form RNA loops to interact with the DNA-dependent RNA polymerase (Cagliero et al., 2014; Das, 1993). Our RNA-seq analysis did not point towards the altered expression of *nusA* and *nusB* in the RNase III mutant, making it unlikely that a transcription read-through caused by the *nus* system *in trans* is responsible for the measured enrichment of RNA directly downstream of the rRNA operons.

The proper processing of rRNA ensures maturation of the precursors to functional end products (some tRNA genes are co-transcribed with the 16S, 23S and 5S rRNA genes), involves several ribonucleases like RNase E, RNase J, YbeY, and RNase III (reviewed in Deutscher, 2009; Srivastava & Schlessinger, 1990) and occurs simultaneously during transcription (French & Miller, 1989). The important role of RNase III in the processing the rRNA transcript to 23S, 16S and 5S rRNAs is well established as well and its role in further rRNA fragmentation α-proteobacteria is well recognised (Apirion et al., 1976; Evguenieva-Hackenberg, 2005; King et al., 1984). As seen in Figure S2 of our study, this process is strictly RNase III-dependent in *R. sphaeroides*. Therefore, it is conceivable that the lack of 23S rRNA fragmentation is affecting rRNA transcription termination via a yet unknown mechanism *in cis*, for example, by altering the RNA secondary structure and transcription rate. YbeY is another endoribonuclease conserved in many bacteria and reported to participate in rRNA processing. In *E. coli*, a deletion of *ybeY* led to the generation of immature 16S rRNA, aberrant ribosome biogenesis, and impaired rRNA transcription anti-termination (Davies

et al., 2010; Grinwald & Ron, 2013; Jacob et al., 2013). However, we did not see an effect of YbeY on the transcript levels downstream of the rRNA operons when testing total RNA samples from an *R. sphaeroides* Δ*ybeY* mutant (Spanka & Klug, 2021) by qRT-PCR (data not shown).

The transcriptome-wide mapping of RNase III cleavage sites revealed a lower number of identified sites compared to our previous mapping of RNase E cleavage sites (between 565 and 2220 cleavage sites found for RNase III, compared to 2007–4206 cleavage sites found for RNase E), which suggests a weaker global regulatory role of RNase III in comparison to RNase E in *R. sphaeroides*. This is in agreement with the number of mRNAs with changed levels in the two strains and with the drastic effect of the *rne* mutation during phototrophic growth (Börner et al., 2023; Förstner et al., 2018).

Loss of RNase III activity caused some clear phenotypic effects in *R. sphaeroides*: reduced pigmentation, alteration of stress resistance and of the quorum-sensing regulatory circuit. Strongly reduced pigmentation occurred especially under microaerobic conditions (Figure 2), when photopigments and photosynthesis complexes are already produced but not necessary for ATP generation (Gregor & Klug, 1999). Under phototrophic conditions, this effect was less pronounced, although photosynthesis complexes are necessary for ATP production (Figure 1).

Our global gene expression analysis of the RNase III mutant did not point towards generally reduced mRNA levels of photosynthesis-related genes (e.g. *crt* and *bch* genes for carotenoid and bacteriochlorophyll synthesis, and *puf* or *puc* genes encoding pigment-binding proteins), as it was recently reported for the *R. sphaeroides* rne^{ts} mutant with reduced RNase E activity (Börner et al., 2023). While we observed decreased mRNA abundances of some known regulators of photosynthesis gene expression in our recent study of the rne^{ts} mutant, our data for the RNase III mutant revealed increased mRNAs levels for the photosynthesis regulators AppA, PpsR and FnrL in the *rnc* mutant under microaerobic and phototrophic conditions (Figures S7a,b and S8). The PpsR/AppA repressor/antirepressor system regulates many photosynthesis genes in response to light and oxygen (Braatsch et al., 2002; Gomelsky & Kaplan, 1997; Han et al., 2007; Masuda & Bauer, 2002), among them also *bch* and *crt* genes. The redox-responsive FnrL also affects the expression of many photosynthesis genes (Imam et al., 2014).

We recently showed that the small RNA-binding DUF1127-domain protein CcaF1 promotes the formation of photosynthesis complexes in *R. sphaeroides* (Grützner et al., 2023). *ccaF1* is co-transcribed with the CcsR sRNAs and also shows higher levels in the rnc^{-} mutant. This excludes the possibility that diminished pigmentation in the mutant strain is due to reduced *ccaF1* transcript levels. Taken together, our RNA-seq data cannot unequivocally explain the effect of RNase III on pigmentation. However, the formation of photosynthetic complexes includes many regulatory circuits (Eisenhardt et al., 2018, 2021; Mank et al., 2012; Reuscher & Klug, 2021) and its regulation is very complex and may also involve yet unknown factors.

A functional role of RNases in the stress response of numerous microorganisms has been reported already in the past. Often a reduction or lack of the native RNase activity leads to enhanced susceptibility towards various cellular stresses, like oxidative, osmotic or temperature stress (Duggal et al., 2020; Förstner et al., 2018; Lejars & Hajnsdorf, 2022; Möller et al., 2019; Spanka et al., 2021). In contrast, our data (Figure 9) document a higher resistance of *R. sphaeroides* against oxidative stress when RNase III activity is lacking. Interestingly, we observed that the higher resistance of the mutant against oxidative stress is accompanied by elevated CcsR levels. The northern blot data (Figure 8) show that the rnc^{-} mutant accumulates CcsR1, compared to the wild type, under non-stress conditions and all tested oxidative stress conditions, but not during heat shock, where expression of CcsR1 was lower than in the wild type. As reported in our previous studies (Billenkamp et al., 2015; Grützner, Billenkamp, et al., 2021), CcsR has an important function in the oxidative stress response of *R. sphaeroides* by affecting glutathione levels through direct binding to *flhR* mRNA encoding a transcriptional activator. Additionally, enrichment of CcsR indirectly decreases the levels of mRNAs encoding subunits of the pyruvate dehydrogenase complex, which is a primary target of reactive oxygen species (ROS) (Billenkamp et al., 2015). It is likely that the enhanced stress resistance against the tested ROS-inducing agents is caused by an accumulation of CcsR. This is supported by the observation that the cell survival rate and CcsR abundance are not affected by RNase III upon heat stress. Furthermore, our results show that the higher levels of CcsR in the mutant are rather due to an increased transcription rate (Figure 7c) than to increased sRNA stability (Figure 8), suggesting an indirect regulatory effect of RNase III on CcsR expression. Presumably, the elevated *rpoE* and *rpoHII* mRNA levels (Figure S5) in the mutant contribute to the higher CcsR abundance.

In a previous study, we could show that RSP_0557, another small protein with DUF1127 domain expressed from a different locus than *ccaF1-ccsR*, has RNA-binding activity and interacts with CcsR transcripts and other RNAs in *R. sphaeroides* (Grützner, Billenkamp, et al., 2021). Our RNA-seq data showed increased mRNA abundances of *RSP_0557* in the RNase III mutant compared to the wild type, under all three growth conditions (Figure S9). The enrichment was further validated by qRT-PCR under microaerobic conditions ($\log_2$ fold change mutant/wt ≈ 1.6). Therefore, it is conceivable that also an increased level of RSP_0557 influences CcsR expression, e.g. by altering the maturation efficiency of *ccaF1-ccsR* precursor transcript to mature CcsR sRNAs.

Since catalases are known to degrade hydrogen peroxide to water and molecular oxygen, and the mutant strain did show increased resistance against hydrogen peroxide, it can be assumed that the enrichment of *catA* mRNA in the mutant positively contributes to the increased survival rate under this specific stress conditions. However, catalases have been reported to be highly specific to hydrogen peroxide and are not expected to accept organic peroxides as a substrate. In a conclusion, the increased survival rate of the rnc^{-} mutant under tBOOH stress can probably not be explained solely by an elevated catalase level. Like the formation of photosynthesis complexes, the oxidative stress response of

R. sphaeroides includes a complex network of different regulators (Eisenhardt et al., 2021).

Strikingly, we found a novel physiological function of RNase III in the regulation of quorum sensing, by controlling the expression of the autoinducer synthase (*cerI*). For RNase E, another important endoribonuclease which is essential in many gram-negative bacteria, an impact on the expression of the autoinducer synthase is already well described (e.g. in the closely related α-proteobacterium *S. meliloti* (Baumgardt et al., 2014)). In our study on *R. sphaeroides*, qRT-PCR (Figure 10) and RNA-seq (read coverage shown in Figure S6) independently confirmed the enrichment of *cerI* mRNA in the *rnc*$^-$ mutant strain, indicating an action of RNase III on the Lux-type QS system. Analysis of the *cerI* mRNA half-life (Figure 10c) revealed increased stability in the mutant strain. Interestingly, we were able to show that RNase III deficiency leads to hyperproduction of AHLs in *R. sphaeroides* (Figure 10a), probably through the enrichment of *cerI* mRNA thus accumulating CerI enzyme in the mutant. For the second component of the *R. sphaeroides* Lux-type system, the signal receptor *cerR*, we did not observe an mRNA enrichment (Figure 10b). As the Lux-type QS system represents a positive feed-forward loop, where AHLs bind to *cerR* and as a complex activate transcription of *cerI*, it is conceivable that also *cerR* is differentially expressed at high AHL concentrations. However, as *cerR* is preceded by its own promoter and we did not find any relevant increase or decrease in *cerR* abundance, we conclude that the transcription of *cerR* is regulated independently of the transcription of *cerI*. Interestingly, we were able to map several bona fide RNase III cleavage sites inside the open reading frame of the *cerI* mRNA as seen in Figure S6 (three under aerobic conditions, one under aerobic conditions), which could account for the measured stabilisation and accumulation of *cerI* mRNA in the *rnc*$^-$ mutant (Figure 10b,c).

Not all *rnc*-dependent effects observed in our transcriptome analysis may be a direct consequence of RNase III cleavage. This can also be seen in a correlation analysis (Figure S10), where we plotted all annotated RNAs from the RNA-seq analysis according to their expression change against the amount of mapped bona fide RNase III cleavage sites. As we observed a widespread expression change of RNAs without mapped cleavage sites, only a slight tendency towards reduced abundance in the mutant was visible for RNAs harbouring mapped cleavage sites. In addition, RNAs with increased amount of mapped cleavage sites showed an unaffected ($\log_2$ fold change mutant/wt of nearly 0) or even increased abundance in the mutant.

On one hand, RNase III directly affects, for example, mRNAs for transcriptional regulators or regulatory small RNAs that in turn will regulate the expression of other genes. Furthermore, as described in the introduction, RNase III is known to regulate the expression of *pnp* for PNPase, which acts as a 3′ to 5′ exoribonuclease. Lack of RNase III activity leads to changed *pnp* levels in *R. sphaeroides* and also to changed *rne* levels (as seen per DESeq2 analysis in Supplementary Tables S3 and S4). We have previously shown that also PNPase and RNase E have strong effects on the *R. sphaeroides* transcriptome and influence stress resistance (Förstner et al., 2018; Spanka et al., 2021). As previous publications, this study emphasises the important role of RNases in bacterial gene regulation.

4 | EXPERIMENTAL PROCEDURES

4.1 | Cultivation of bacterial strains

R. sphaeroides and *Sinorhizobium meliloti* were cultivated in malate minimal medium (Remes et al., 2014) at 32°C. Cultivation of *Escherichia coli* S17-1 (Simon et al., 1983) for cloning procedures and diparental conjugation (Klug & Drews, 1984) was performed in standard I medium (Roth) at 37°C and 180 rpm. *R. sphaeroides* strains were grown either at a high oxygen concentration of 160–180 μM dissolved oxygen (aerobic cultures), low oxygen concentration of 25–30 μM dissolved oxygen (microaerobic cultures) or anaerobically with 60 $W * m^{-2}$ white light (phototrophic cultures).

For determination of RNA half-lives, 0.2 mg/mL rifampicin (Serva Electrophoresis) was added to exponentially grown biological triplicates of *R. sphaeroides* wild type and *rnc*_GD48,49SR-mutant strain (*rnc*$^-$). Cell samples were collected prior to the addition ($t = 0$ min) and 5, 10, 15, 20 and 25 min afterwards.

For induction of the bacterial stress response, biological triplicates of wild type and mutant strain were grown microaerobically to mid-exponential growth phase followed by incubation in the presence of 0.25 mM paraquat (Sigma-Aldrich), 0.3 mM tBOOH (Sigma-Aldrich), 0.01 mM $CdCl_2$ (Sigma-Aldrich) or 0.5 mM H_2O_2 (Roth) for 20 min prior to sample collection. For heat stress, the exponential cultures were shifted to 42°C for 60 min.

4.2 | Construction of the *R. sphaeroides* RNase III mutant

All oligonucleotides used in this study are listed in Supplementary Table S5. To inactivate the catalytic function of RNase III in *R. sphaeroides*, two relevant amino acids in the active centre of the native enzyme were substituted (G48S, D49R). For this, the whole 690 bp open reading frame of the native RNase III encoding gene (*rnc*) of *R. sphaeroides* 2.4.1 was amplified by PCR using the oligonucleotides rnc_frag_for_BamHI and rnc_frag_rev_KpnI. The resulting amplicon was ligated into the pJet1.2/blunt vector (Thermo Scientific) following the manufacturer's protocol, yielding plasmid pJet-rnc. To mutate the nucleotides of interest within the *rnc* gene by side-directed mutagenesis, plasmid pJet-rnc was amplified by PCR using the oligonucleotides rnc_rolling_for and rnc_rolling_rev, yielding plasmid pJet-rnc-mut. Subsequently, pJet-rnc-mut was restricted using restriction enzymes *Bam*HI and *Xba*I. The resulting 705 bp fragment was electrophoretically separated on a 1% (w/v) agarose TAE gel, extracted using the innuPREP DOUBLEpure kit (Analytik Jena) according to the manufacturer's protocol, and inserted into the suicide vector pK18mobII-*sacB* (Schäfer et al., 1994) by *Bam*HI and

*Xba*I, yielding plasmid pK18-rnc-mut. Subsequently, pK18-rnc-mut was transferred in *R. sphaeroides* 2.4.1 wild type by diparental conjugation with *E. coli* S17-1 and used for chromosomal integration via homologous recombination (double cross-over).

For complementation of the RNase III deficiency, the native *rnc* gene was cloned under transcriptional control of the native *lep-rnc-era* promoter on the expression vector pRK4352 (Mank et al., 2012). The 400 bp promoter region directly upstream of the *lep* gene was amplified by PCR using the oligonucleotides Prnc_for_HindIII and Prnc_rev_BamHI. The resulting amplicon was inserted to pRK4352 via *Hin*dIII and *Bam*HI, followed by insertion of the previously generated *rnc* containing 690 bp fragment via *Bam*HI and *Kpn*I, yielding plasmid pRK-*rnc*. pRK-*rnc* was transferred to the *R. sphaeroides* RNase III mutant by diparental conjugation using *E. coli* S17-1.

To insert additional transcription terminators directly downstream to the rRNA operons within the *rnc*$^-$ mutant, we cloned three DNA fragments for homologues recombination into modified pK18 plasmids, pK1.2 (Kretz et al., 2023), harbouring an array of four *rrnB* T1 transcription terminators (Ham et al., 2006). The three fragments for homologues recombination were amplified from genomic DNA of *R. sphaeroides* 2.4.1 by PCR using oligonucleotide pairs Term1_for_HindIII and Term1_rev_XbaI, Term2_for_HindIII and Term2_rev_XbaI and Term3_for_HindIII and Term3_rev_XbaI. Subsequently, the amplicons were inserted into pK1.2 with *Hin*dIII and *Xba*I. The resulting plasmids were transferred to the *R. sphaeroides rnc*$^-$ strain by diparental conjugation using *E. coli* S17-1 followed by chromosomal integration via homologues recombination (single cross-over), introducing the *rrnB* T1 transcription terminator array at the targeted sequences downstream of the *R. sphaeroides* rRNA operons.

4.3 | Analysis of photopigments

Biological triplicates of wild type and *rnc*$^-$ mutant were grown under microaerobic or phototrophic conditions to mid-exponential growth phase. Cells from 1 mL of culture were sedimented by centrifugation for 10 min at 8000 rpm and cell pellets were resuspended in 50 µL ddH_2O. 500 µL acetone/methanol (7:2, v/v) were added to extract the photopigments. Cell debris was removed by centrifugation for 5 min at 13,000 rpm, and the supernatant was used for absorbance measurements at $\lambda = 770$ nm (bacteriochlorophyll a) and $\lambda = 585$ nm (carotenoids). Concentrations were calculated using the extinction coefficient 76 $mM^{-1} cm^{-1}$ (bacteriochlorophyll a) or 128 $mM^{-1} cm^{-1}$ (carotenoids).

For analysis of whole-cell spectra, 800 µL cell culture samples were collected, and the absorbance values between $\lambda = 400$ nm and $\lambda = 900$ nm were measured on a spectrophotometer (Specord 50, Analytik Jena) and subsequently normalised to OD_{660}.

4.4 | Assessment of bacterial stress resistance

For survival assays, biological triplicates of wild type and *rnc*$^-$ mutant were grown microaerobically to mid-exponential growth phase. The bacterial stress response was induced as described above. 10^{-5} dilutions of the cultures were plated on malate minimal agar plates and incubated for 48 h at 32°C. Colony-forming units per mL were calculated, and the survival rate at 32°C without stress agents was used as a reference.

The zone of inhibition assay was performed as described previously (Grützner, Billenkamp, et al., 2021). 5 µL of 0.1 M $CdCl_2$, 0.5 M tBOOH, 1 M H_2O_2 and 0.01 M methylene blue were spotted on the filter discs. The agar plates were either incubated in the dark or illuminated with 85 µmol $m^{-2} s^{-1}$ white light (only for plates treated with methylene blue).

4.5 | AHL measurements

To assess concentrations of secreted AHLs from *R. sphaeroides* wild type and *rnc*$^-$ mutant, a previously established *S. meliloti* reporter strain (McIntosh et al., 2019) was used, that carries a transcriptional fusion of the SMb20911 promoter (promoter controlling the transcription of an uncharacterised small open reading frame in *S. meliloti* 1021) and the mVenus gene on a low copy plasmid. Since the SMb20911 promoter is fully active in the absence of AHLs and becomes repressed by rising AHL concentration, the resulting mVenus fluorescence (extinction: 515 nm; emission: 548 nm) is negatively correlated to the applied AHL concentration.

The *S. meliloti* reporter strain was grown in malate minimal medium and increasing amounts (0%–100%) of cell-free supernatant from microaerobically grown *R. sphaeroides* wild type cultures, to assess the correlation between autoinducer concentration and reduction of mVenus signal. To quantify the secreted AHL amounts of the *R. sphaeroides rnc*$^-$ strain, biological triplicates of the *S. meliloti* reporter strain were cultivated in 25% cell-free supernatant from the microaerobically grown *R. sphaeroides rnc*$^-$ strain and malate minimal medium. A reporter culture grown in malate minimal medium with 400 nM commercially obtained oxo-C16:1-HL (N-3-oxo-hexadec-11(Z)-enoyl-L-homoserine lactone; Cayman Chemical) served as reference.

4.6 | Quantification of RNA abundances

RNA isolation was performed as described previously (Börner et al., 2023), using the hot phenol technique (Damm et al., 2015; Janzon et al., 1986).

For northern blot analysis, either 7 µg or 10 µg total RNA was electrophoretically separated on denaturing 10% polyacrylamide gels, transferred to 0.45 µM nylon membranes by semidry electroblotting and subsequently immobilised by UV crosslinking. For specific detection, immobilised RNAs were hybridised with radiolabelled antisense DNA oligonucleotides (listed in Supplementary Table S5) in Church buffer with low stringency (Church & Gilbert, 1984). After hybridisation, membranes were washed with 5× SSC buffer containing 0.01% SDS twice under rotation

at 42°C, dried and exposed to a phosphor imaging screen (Bio-Rad). Phosphor imaging signals were evaluated using the Quantity One® 1-D analysis software (Bio-Rad). For removal of the hybridised DNA oligonucleotides, membranes were incubated in 5× SSC buffer containing 0.1% SDS for 20 min at 95°C and 80 rpm. 3′ end labelling of DNA oligonucleotides was performed using [γ-^{32}P] ATP (Hartmann Analytic) and T4 polynucleotide kinase (NEB) following the manufacturer's protocol.

Quantitative-reverse transcriptase PCR (qRT-PCR) and RNA sequencing of DNA-free total RNA were performed as described in Börner et al., 2023. The oligonucleotides used for qRT-PCR are listed in Supplementary Table S5.

4.7 | Bioinformatics analysis

Samples from biological triplicates of wild type and *rnc*$^-$-mutant strains, grown under aerobic, microaerobic or phototrophic growth conditions, were analysed by RNA sequencing. Raw sequencing data were aligned to the reference genome of *R. sphaeroides* (NC_007493.2, NC_007494.2, NC_009007.1, NC_007488.2, NC_007489.1, NC_007490.2 and NC_009008.1), saved as binary alignment maps (BAM) files and converted to coverage tracks (wiggle) using the READemption pipeline (Förstner et al., 2014) v.1.0.5. Wiggle files for the individual samples that belong to the same condition were merged within R v.4.1.2 using rtracklayer v.1.56.1 (Lawrence et al., 2009). Read counts per gene were identified using the summarize Overlaps function (Lawrence et al., 2013) based on the BAM files and the gene transfer file (GTF) file of *R. sphaeroides*. Transcriptome changes between the growth conditions (aerobic, microaerobic or phototrophic) were individually calculated for the wild type and *rnc*$^-$ mutant using DESeq2 v. 1.32 (Love et al., 2014). In order to identify differentially expressed genes between wild type and mutant, the individual significantly differentially regulated genes ($\log_2$ fold change >1 or <−1, adjusted *p*-value <0.05, mean of read counts >10) of both wild type and mutant between different growth conditions were plotted as heat maps. These heat maps were unsupervised agglomerative hierarchical clustered to reveal different expression patterns between wild type and mutant.

Identification and annotation of bona fide cleavage sites were previously described in detail (Börner et al., 2023). In short, strand-specific 5′ counts were compared between wild type and mutant using DESeq2 v.1.32 and subsequently filtered for minimal counts of >10, $\log_2$ fold change >1 and adjusted *p*-value <0.05. Multiple 5′ ends that fulfil all criteria and were localised within three base positions adjacent to each other were merged. Annotation of the features associated with cleavage sites was performed based on the *R. sphaeroides* GTF file using the GenomicRanges (Lawrence et al., 2013) package.

In order to compare the transcriptomic effects of RNase III between *R. sphaeroides* and *E. coli*, raw RNA-seq reads from *E. coli* wild type and RNase III mutant were downloaded from the ArrayExpress repository (accession number: E-MTAB-9507). These raw reads were aligned against the K12 DH10B *E. coli* reference genome and coverage tracks (wiggle) were generated using READemption v.1.0.5.

4.8 | RNase III activity reporter assay

To investigate the RNase III activity in vivo, a new reporter plasmid similar to our previously described construct for assaying RNase E activity (Börner et al., 2023) was generated. For this, we introduced the well-known RNase III cleavage site of the native pre-16S rRNA into the previously constructed pPHU231-p16S-mVenus plasmid (Börner et al., 2023).

The 82 bp genomic sequence of the pre-16S rRNA cleavage site was amplified by PCR using oligonucleotides 5′_16S_for_ScaI and 5′_16S_rev_XbaI, followed by insertion into pPHU231-p16S-mVenus via *Sca*I and *Xba*I yielding plasmid pPHU231-5′UTR-mVenus (indicator plasmid). Subsequently, the plasmid was transferred to *rnc*$^-$ and wild type cells by diparental conjugation using the *E. coli* S17-1 strain.

Cultivation of the conjugants and measurements of the resulting mVenus fluorescence were performed as described previously (Börner et al., 2023). As a reference, the mVenus fluorescence generated by the wild type and *rnc*$^-$ strain carrying the control plasmid (pPHU231-p16S-mVenus) was analysed.

AUTHOR CONTRIBUTIONS

Gabriele Klug: Methodology; conceptualization; funding acquisition; writing – original draft; writing – review and editing; data curation; supervision; formal analysis; project administration; resources. **Janek Börner:** Conceptualization; methodology; investigation; writing – original draft; writing – review and editing; validation; data curation; visualization; project administration; formal analysis. **Tobias Friedrich:** Investigation; writing – review and editing; visualization; data curation; formal analysis; software.

ACKNOWLEDGEMENTS

We thank Kerstin Haberzettl and Andrea Weisert for excellent technical assistance with DNA cloning procedures, Florian Gerken and Fabian Droß for experimental support, Florian Leinberger for assistance with RNA-seq cross-sample normalisation and Matthew McIntosh for help and fruitful discussions concerning the quorum-sensing system investigations. This work was funded by Deutsche Forschungsgemeinschaft (DFG KI563/41-1). Open Access funding enabled and organized by Projekt DEAL.

CONFLICT OF INTEREST STATEMENT

None declared.

DATA AVAILABILITY STATEMENT

The RNA-seq data analysed in this study are publicly available in the NCBI Gene Expression Omnibus (GEO, https://www.ncbi.nlm.nih.gov/geo/) repository with the accession numbers GSE200990 (wild type samples) and GSE236804 (RNase III mutant samples).

ETHICS STATEMENT

The authors declare that no human or animal subjects were used in this study.

ORCID

Janek Börner https://orcid.org/0000-0003-4824-9393
Tobias Friedrich https://orcid.org/0000-0003-4014-8678
Gabriele Klug https://orcid.org/0000-0002-3527-5093

REFERENCES

Adnan, F., Weber, L. & Klug, G. (2015) The sRNA SorY confers resistance during photooxidative stress by affecting a metabolite transporter in *Rhodobacter sphaeroides*. *RNA Biology*, 12, 569–577.

Afonyushkin, T., Vecerek, B., Moll, I., Bläsi, U. & Kaberdin, V.R. (2005) Both RNase E and RNase III control the stability of *sodB* mRNA upon translational inhibition by the small regulatory RNA RyhB. *Nucleic Acids Research*, 33, 1678–1689.

Altuvia, Y., Bar, A., Reiss, N., Karavani, E., Argaman, L. & Margalit, H. (2018) In vivo cleavage rules and target repertoire of RNase III in *Escherichia coli*. *Nucleic Acids Research*, 46, 10380–10394.

Apirion, D., Neil, J. & Watson, N. (1976) Revertants from RNase III negative strains of *Escherichia coli*. *Molecular & General Genetics*, 149, 201–210.

Apirion, D. & Watson, N. (1975) Mapping and characteryation of a mutation in *Escherichia coli* that reduces the level of ribonuclease III specific for double-stranded ribonucleic acid. *Journal of Bacteriology*, 124, 317–324.

Baumgardt, K., Charoenpanich, P., McIntosh, M., Schikora, A., Stein, E., Thalmann, S. et al. (2014) RNase E affects the expression of the acyl-homoserine lactone synthase gene *sinI* in *Sinorhizobium meliloti*. *Journal of Bacteriology*, 196, 1435–1447.

Belasco, J.G. & Brawerman, G. (Eds.). (1993) *Control of messenger RNA stability*. New York, NY: Academic Press.

Berghoff, B.A., Glaeser, J., Sharma, C.M., Vogel, J. & Klug, G. (2009) Photooxidative stress-induced and abundant small RNAs in *Rhodobacter sphaeroides*. *Molecular Microbiology*, 74, 1497–1512.

Billenkamp, F., Peng, T., Berghoff, B.A. & Klug, G. (2015) A cluster of four homologous small RNAs modulates C1 metabolism and the pyruvate dehydrogenase complex in *Rhodobacter sphaeroides* under various stress conditions. *Journal of Bacteriology*, 197, 1839–1852.

Blomberg, P., Wagner, E.G. & Nordström, K. (1990) Control of replication of plasmid R1: the duplex between the antisense RNA, CopA, and its target, CopT, is processed specifically in vivo and in vitro by RNase III. *The EMBO Journal*, 9, 2331–2340.

Boisset, S., Geissmann, T., Huntzinger, E., Fechter, P., Bendridi, N., Possedko, M. et al. (2007) *Staphylococcus aureus* RNAIII coordinately represses the synthesis of virulence factors and the transcription regulator Rot by an antisense mechanism. *Genes & Development*, 21, 1353–1366.

Börner, J., Friedrich, T., Bartkuhn, M. & Klug, G. (2023) Ribonuclease E strongly impacts bacterial adaptation to different growth conditions. *RNA Biology*, 20, 120–135.

Braatsch, S., Gomelsky, M., Kuphal, S. & Klug, G. (2002) A single flavoprotein, AppA, integrates both redox and light signals in *Rhodobacter sphaeroides*. *Molecular Microbiology*, 45, 827–836.

Cagliero, C., Zhou, Y.N. & Jin, D.J. (2014) Spatial organization of transcription machinery and its segregation from the replisome in fast-growing bacterial cells. *Nucleic Acids Research*, 42, 13696–13705.

Carmell, M.A. & Hannon, G.J. (2004) RNase III enzymes and the initiation of gene silencing. *Nature Structural & Molecular Biology*, 11, 214–218.

Carzaniga, T., Briani, F., Zangrossi, S., Merlino, G., Marchi, P. & Dehò, G. (2009) Autogenous regulation of *Escherichia coli* polynucleotide phosphorylase expression revisited. *Journal of Bacteriology*, 191, 1738–1748.

Church, G.M. & Gilbert, W. (1984) Genomic sequencing. *Proceedings of the National Academy of Sciences of the United States of America*, 81, 1991–1995.

Conrad, S.E. & Campbell, J.L. (1979) Role of plasmid-coded RNA and ribonuclease III in plasmid DNA replication. *Cell*, 18, 61–71.

Cortez, N., Carrillo, N., Pasternak, C., Balzer, A. & Klug, G. (1998) Molecular cloning and expression analysis of the *Rhodobacter capsulatus sodB* gene, encoding an iron superoxide dismutase. *Journal of Bacteriology*, 180, 5413–5420.

Court, D.L., Gan, J., Liang, Y.-H., Shaw, G.X., Tropea, J.E., Costantino, N. et al. (2013) RNase III: genetics and function; structure and mechanism. *Annual Review of Genetics*, 47, 405–431.

Damm, K., Bach, S., Müller, K.M.H., Klug, G., Burenina, O.Y., Kubareva, E.A. et al. (2015) Impact of RNA isolation protocols on RNA detection by Northern blotting. *Methods in Molecular Biology (Clifton, N.J.)*, 1296, 29–38.

Das, A. (1993) Control of transcription termination by RNA-binding proteins. *Annual Review of Biochemistry*, 62, 893–930.

Dasgupta, S., Fernandez, L., Kameyama, L., Inada, T., Nakamura, Y., Pappas, A. et al. (1998) Genetic uncoupling of the dsRNA-binding and RNA cleavage activities of the *Escherichia coli* endoribonuclease RNase III—the effect of dsRNA binding on gene expression. *Molecular Microbiology*, 28, 629–640.

Davies, B.W., Köhrer, C., Jacob, A.I., Simmons, L.A., Zhu, J., Aleman, L.M. et al. (2010) Role of *Escherichia coli* YbeY, a highly conserved protein, in rRNA processing. *Molecular Microbiology*, 78, 506–518.

DeRosa, M.C. & Crutchley, R.J. (2002) Photosensitized singlet oxygen and its applications. *Coordination Chemistry Reviews*, 233, 351–371.

Deutscher, M.P. (2009) Maturation and degradation of ribosomal RNA in bacteria. *Progress in Molecular Biology and Translational Science*, 85, 369–391.

Dufour, Y.S., Imam, S., Koo, B.-M., Green, H.A. & Donohue, T.J. (2012) Convergence of the transcriptional responses to heat shock and singlet oxygen stresses. *PLoS Genetics*, 8, e1002929.

Duggal, Y., Fontaine, B.M., Dailey, D.M., Ning, G. & Weinert, E.E. (2020) RNase I modulates *Escherichia coli* motility, metabolism, and resistance. *ACS Chemical Biology*, 15, 1996–2004.

Dunn, J.J. & Studier, F.W. (1973) T7 early RNAs and *Escherichia coli* ribosomal RNAs are cut from large precursor RNAs in vivo by ribonuclease 3. *Proceedings of the National Academy of Sciences of the United States of America*, 70, 3296–3300.

Eisenhardt, K.M.H., Remes, B., Grützner, J., Spanka, D.-T., Jäger, A. & Klug, G. (2021) A complex network of sigma factors and sRNA StsR regulates stress responses in *R. sphaeroides*. *International Journal of Molecular Sciences*, 22, 7557.

Eisenhardt, K.M.H., Reuscher, C.M. & Klug, G. (2018) PcrX, an sRNA derived from the 3′- UTR of the *Rhodobacter sphaeroides puf* operon modulates expression of *puf* genes encoding proteins of the bacterial photosynthetic apparatus. *Molecular Microbiology*, 110, 325–334.

Engebrecht, J. & Silverman, M. (1984) Identification of genes and gene products necessary for bacterial bioluminescence. *Proceedings of the National Academy of Sciences of the United States of America*, 81, 4154–4158.

Evguenieva-Hackenberg, E. (2005) Bacterial ribosomal RNA in pieces. *Molecular Microbiology*, 57, 318–325.

Evguenieva-Hackenberg, E. & Klug, G. (2000) RNase III processing of intervening sequences found in helix 9 of 23S rRNA in the alpha subclass of *Proteobacteria*. *Journal of Bacteriology*, 182, 4719–4729.

Förstner, K.U., Reuscher, C.M., Haberzettl, K., Weber, L. & Klug, G. (2018) RNase E cleavage shapes the transcriptome of *Rhodobacter*

sphaeroides and strongly impacts phototrophic growth. *Life Science Alliance*, 1, e201800080.

Förstner, K.U., Vogel, J. & Sharma, C.M. (2014) READemption-a tool for the computational analysis of deep-sequencing-based transcriptome data. *Bioinformatics*, 30, 3421–3423.

Freese, N.H., Norris, D.C. & Loraine, A.E. (2016) Integrated genome browser: visual analytics platform for genomics. *Bioinformatics*, 32, 2089–2095.

French, S.L. & Miller, O.L. (1989) Transcription mapping of the *Escherichia coli* chromosome by electron microscopy. *Journal of Bacteriology*, 171, 4207–4216.

Fuqua, W.C., Winans, S.C. & Greenberg, E.P. (1994) Quorum sensing in bacteria: the LuxR-LuxI family of cell density-responsive transcriptional regulators. *Journal of Bacteriology*, 176, 269–275.

Gatewood, M.L., Bralley, P. & Jones, G.H. (2011) RNase III-dependent expression of the *rpsO-pnp* operon of *Streptomyces coelicolor*. *Journal of Bacteriology*, 193, 4371–4379.

Gatewood, M.L., Bralley, P., Weil, M.R. & Jones, G.H. (2012) RNA-Seq and RNA immunoprecipitation analyses of the transcriptome of *Streptomyces coelicolor* identify substrates for RNase III. *Journal of Bacteriology*, 194, 2228–2237.

Gerdes, K., Nielsen, A., Thorsted, P. & Wagner, E.G. (1992) Mechanism of killer gene activation. Antisense RNA-dependent RNase III cleavage ensures rapid turn-over of the stable *hok*, *srnB* and *pndA* effector messenger RNAs. *Journal of Molecular Biology*, 226, 637–649.

Gomelsky, M. & Kaplan, S. (1997) Molecular genetic analysis suggesting interactions between AppA and PpsR in regulation of photosynthesis gene expression in *Rhodobacter sphaeroides* 2.4. 1. *Journal of Bacteriology*, 179, 128–134.

Greenberg, E.P., Hastings, J.W. & Ulitzur, S. (1979) Induction of luciferase synthesis in *Beneckea harveyi* by other marine bacteria. *Archives of Microbiology*, 120, 87–91.

Gregor, J. & Klug, G. (1999) Regulation of bacterial photosynthesis genes by oxygen and light. *FEMS Microbiology Letters*, 179, 1–9.

Grinwald, M. & Ron, E.Z. (2013) The *Escherichia coli* translation-associated heat shock protein YbeY is involved in rRNA transcription antitermination. *PLoS ONE*, 8, e62297.

Grützner, J., Billenkamp, F., Spanka, D.-T., Rick, T., Monzon, V., Förstner, K.U. et al. (2021) The small DUF1127 protein CcaF1 from *Rhodobacter sphaeroides* is an RNA-binding protein involved in sRNA maturation and RNA turnover. *Nucleic Acids Research*, 49, 3003–3019.

Grützner, J., Börner, J., Jäger, A. & Klug, G. (2023) The small RNA-binding protein CcaF1 promotes formation of photosynthetic complexes in *Rhodobacter sphaeroides*. *International Journal of Molecular Sciences*, 24, 9515.

Grützner, J., Remes, B., Eisenhardt, K.M.H., Scheller, D., Kretz, J., Madhugiri, R. et al. (2021) sRNA-mediated RNA processing regulates bacterial cell division. *Nucleic Acids Research*, 49, 7035–7052.

Ham, T.S., Lee, S.K., Keasling, J.D. & Arkin, A.P. (2006) A tightly regulated inducible expression system utilizing the *fim* inversion recombination switch. *Biotechnology and Bioengineering*, 94, 1–4.

Han, Y., Meyer, M.H., Keusgen, M. & Klug, G. (2007) A haem cofactor is required for redox and light signalling by the AppA protein of *Rhodobacter sphaeroides*. *Molecular Microbiology*, 64, 1090–1104.

Hördt, A., López, M.G., Meier-Kolthoff, J.P., Schleuning, M., Weinhold, L.-M., Tindall, B.J. et al. (2020) Analysis of 1,000+ type-strain genomes substantially improves taxonomic classification of *alphaproteobacteria*. *Frontiers in Microbiology*, 11, 468.

Huntzinger, E., Boisset, S., Saveanu, C., Benito, Y., Geissmann, T., Namane, A. et al. (2005) *Staphylococcus aureus* RNAIII and the endoribonuclease III coordinately regulate *spa* gene expression. *The EMBO Journal*, 24, 824–835.

Ifill, G., Blimkie, T., Lee, A.H.Y., Mackie, G.A., Chen, Q., Stibitz, S. et al. (2021) RNase III and RNase E influence posttranscriptional regulatory networks involved in virulence factor production, metabolism, and regulatory RNA processing in *Bordetella pertussis*. *mSphere*, 6, 10–1128.

Imam, S., Noguera, D.R. & Donohue, T.J. (2014) Global analysis of photosynthesis transcriptional regulatory networks. *PLoS Genetics*, 10, e1004837.

Jacob, A.I., Köhrer, C., Davies, B.W., RajBhandary, U.L. & Walker, G.C. (2013) Conserved bacterial RNase YbeY plays key roles in 70S ribosome quality control and 16S rRNA maturation. *Molecular Cell*, 49, 427–438.

Janzon, L., Löfdahl, S. & Arvidson, S. (1986) Evidence for a coordinate transcriptional control of alpha-toxin and protein a synthesis in *Staphylococcus aureus*. *FEMS Microbiology Letters*, 33(2–3), 193–198.

Jørgensen, M.G., Pettersen, J.S. & Kallipolitis, B.H. (2020) sRNA-mediated control in bacteria: an increasing diversity of regulatory mechanisms. *Biochimica et Biophysica Acta (BBA) - Gene Regulatory Mechanisms*, 1863, 194504.

Kang, H. & Hata, A. (2012) Control of Drosha-mediated microRNA maturation by smad proteins. In: *Eukaryotic RNases and their partners in RNA degradation and biogenesis, part B*. New York, NY: Elsevier, pp. 123–136.

Kindler, P., Keil, T.U. & Hofschneider, P.H. (1973) Isolation and characterization of a ribonuclease 3 deficient mutant of *Escherichia coli*. *Molecular & General Genetics*, 126, 53–59.

King, T.C., Sirdeshmukh, R. & Schlessinger, D. (1984) RNase III cleavage is obligate for maturation but not for function of *Escherichia coli* pre-23S rRNA. *Proceedings of the National Academy of Sciences of the United States of America*, 81, 185–188.

Klug, G. & Drews, G. (1984) Construction of a gene bank of *Rhodopseudomonas capsulata* using a broad host range DNA cloning system. *Archives of Microbiology*, 139, 319–325.

Kretz, J., Israel, V. & McIntosh, M. (2023) Design–build–test of synthetic promoters for inducible gene regulation in alphaproteobacteria. *ACS Synthetic Biology.*, 12, 2663–2675.

Lalaouna, D., Baude, J., Wu, Z., Tomasini, A., Chicher, J., Marzi, S. et al. (2019) RsaC sRNA modulates the oxidative stress response of *Staphylococcus aureus* during manganese starvation. *Nucleic Acids Research*, 47, 9871–9887.

Lawrence, M., Gentleman, R. & Carey, V. (2009) rtracklayer: an R package for interfacing with genome browsers. *Bioinformatics*, 25, 1841–1842.

Lawrence, M., Huber, W., Pagès, H., Aboyoun, P., Carlson, M., Gentleman, R. et al. (2013) Software for computing and annotating genomic ranges. *PLoS Computational Biology*, 9, e1003118.

Lejars, M. & Hajnsdorf, E. (2022) RNase III participates in the adaptation to temperature shock and oxidative stress in *Escherichia coli*. *Microorganisms*, 10, 699.

Lioliou, E., Sharma, C.M., Caldelari, I., Helfer, A.-C., Fechter, P., Vandenesch, F. et al. (2012) Global regulatory functions of the *Staphylococcus aureus* endoribonuclease III in gene expression. *PLoS Genetics*, 8, e1002782.

Love, M.I., Huber, W. & Anders, S. (2014) Moderated estimation of fold change and dispersion for RNA-seq data with DESeq2. *Genome Biology*, 15, 550.

Maes, A., Gracia, C., Innocenti, N., Zhang, K., Aurell, E. & Hajnsdorf, E. (2017) Landscape of RNA polyadenylation in *E. coli*. *Nucleic Acids Research*, 45, 2746–2756.

Mahendran, G., Jayasinghe, O.T., Thavakumaran, D., Arachchilage, G.M. & Silva, G.N. (2022) Key players in regulatory RNA realm of bacteria. *Biochemistry and Biophysics Reports*, 30, 101276.

Mank, N.N., Berghoff, B.A., Hermanns, Y.N. & Klug, G. (2012) Regulation of bacterial photosynthesis genes by the small noncoding RNA PcrZ. *Proceedings of the National Academy of Sciences of the United States of America*, 109, 16306–16311.

Masuda, S. & Bauer, C.E. (2002) AppA is a blue light photoreceptor that antirepresses photosynthesis gene expression in *Rhodobacter sphaeroides*. *Cell*, 110, 613–623.

McIntosh, M., Serrania, J. & Lacanna, E. (2019) A novel LuxR-type solo of *Sinorhizobium meliloti*, NurR, is regulated by the chromosome replication coordinator, DnaA and activates quorum sensing. *Molecular Microbiology*, 112, 678–698.

McKellar, S.W., Ivanova, I., Arede, P., Zapf, R.L., Mercier, N., Chu, L.-C. et al. (2022) RNase III CLASH in MRSA uncovers sRNA regulatory networks coupling metabolism to toxin expression. *Nature Communications*, 13, 3560.

Mediati, D.G., Wong, J.L., Gao, W., McKellar, S., Pang, C.N.I., Wu, S. et al. (2022) RNase III-CLASH of multi-drug resistant *Staphylococcus aureus* reveals a regulatory mRNA 3′ UTR required for intermediate vancomycin resistance. *Nature Communications*, 13, 3558.

Miller, M.B. & Bassler, B.L. (2001) Quorum sensing in bacteria. *Annual Review of Microbiology*, 55, 165–199.

Möller, P., Busch, P., Sauerbrei, B., Kraus, A., Förstner, K.U., Wen, T.-N. et al. (2019) The RNase YbeY is vital for ribosome maturation, stress resistance, and virulence of the natural genetic engineer *Agrobacterium tumefaciens*. *Journal of Bacteriology*, 201, e00730-18.

Müller, K.M.H., Berghoff, B.A., Eisenhardt, B.D., Remes, B. & Klug, G. (2016) Characteristics of Pos19—a small coding RNA in the oxidative stress response of *Rhodobacter sphaeroides*. *PLoS ONE*, 11, e0163425.

Nashimoto, H. & Uchida, H. (1985) DNA sequencing of the *Escherichia coli* ribonuclease III gene and its mutations. *Molecular & General Genetics*, 201, 25–29.

Nealson, K.H., Platt, T. & Hastings, J.W. (1970) Cellular control of the synthesis and activity of the bacterial luminescent system. *Journal of Bacteriology*, 104, 313–322.

Nicholson, A.W. (2014) Ribonuclease III mechanisms of double-stranded RNA cleavage. *Wiley Interdisciplinary Reviews. RNA*, 5, 31–48.

Nikolaev, N., Silengo, L. & Schlessinger, D. (1973) Synthesis of a large precursor to ribosomal RNA in a mutant of *Escherichia coli*. *Proceedings of the National Academy of Sciences of the United States of America*, 70, 3361–3365.

Nuss, A.M., Glaeser, J., Berghoff, B.A. & Klug, G. (2010) Overlapping alternative sigma factor regulons in the response to singlet oxygen in *Rhodobacter sphaeroides*. *Journal of Bacteriology*, 192, 2613–2623.

Nuss, A.M., Glaeser, J. & Klug, G. (2009) RpoH(II) activates oxidative-stress defense systems and is controlled by RpoE in the singlet oxygen-dependent response in *Rhodobacter sphaeroides*. *Journal of Bacteriology*, 191, 220–230.

Opdyke, J.A., Fozo, E.M., Hemm, M.R. & Storz, G. (2011) RNase III participates in GadY-dependent cleavage of the *gadX-gadW* mRNA. *Journal of Molecular Biology*, 406, 29–43.

Papenfort, K. & Melamed, S. (2023) Small RNAs, large networks: post-transcriptional regulons in gram-negative bacteria. *Annual Review of Microbiology*, 77, 23–43.

Peng, T., Berghoff, B.A., Oh, J.-I., Weber, L., Schirmer, J., Schwarz, J. et al. (2016) Regulation of a polyamine transporter by the conserved 3′ UTR-derived sRNA SorX confers resistance to singlet oxygen and organic hydroperoxides in *Rhodobacter sphaeroides*. *RNA Biology*, 13, 988–999.

Portier, C., Dondon, L., Grunberg-Manago, M. & Régnier, P. (1987) The first step in the functional inactivation of the *Escherichia coli* polynucleotide phosphorylase messenger is a ribonuclease III processing at the 5′ end. *The EMBO Journal*, 6, 2165–2170.

Rath, E.C., Pitman, S., Cho, K.H. & Bai, Y. (2017) Identification of streptococcal small RNAs that are putative targets of RNase III through bioinformatics analysis of RNA sequencing data. *BMC Bioinformatics*, 18, 111–120.

Rauhut, R., Jäger, A., Conrad, C. & Klug, G. (1996) Identification and analysis of the *rnc* gene for RNase III in *Rhodobacter capsulatus*. *Nucleic Acids Research*, 24, 1246–1251.

Régnier, P. & Grunberg-Manago, M. (1990) RNase III cleavages in non-coding leaders of *Escherichia coli* transcripts control mRNA stability and genetic expression. *Biochimie*, 72, 825–834.

Remes, B., Berghoff, B.A., Förstner, K.U. & Klug, G. (2014) Role of oxygen and the OxyR protein in the response to iron limitation in *Rhodobacter sphaeroides*. *BMC Genomics*, 15, 794.

Reuscher, C.M. & Klug, G. (2021) Antisense RNA asPcrL regulates expression of photosynthesis genes in *Rhodobacter sphaeroides* by promoting RNase III-dependent turn-over of *puf* mRNA. *RNA Biology*, 18, 1445–1457.

Robertson, H.D., Webster, R.E. & Zinder, N.D. (1967) A nuclease specific for double-stranded RNA. *Virology*, 32, 718–719.

Robertson, H.D., Webster, R.E. & Zinder, N.D. (1968) Purification and properties of ribonuclease III from *Escherichia coli*. *The Journal of Biological Chemistry*, 243, 82–91.

Romby, P., Vandenesch, F. & Wagner, E.G.H. (2006) The role of RNAs in the regulation of virulence-gene expression. *Current Opinion in Microbiology*, 9, 229–236.

Salmond, G.P., Bycroft, B.W., Stewart, G.S. & Williams, P. (1995) The bacterial 'enigma': cracking the code of cell-cell communication. *Molecular Microbiology*, 16, 615–624.

Schäfer, A., Tauch, A., Jäger, W., Kalinowski, J., Thierbach, G. & Pühler, A. (1994) Small mobilizable multi-purpose cloning vectors derived from the *Escherichia coli* plasmids pK18 and pK19: selection of defined deletions in the chromosome of *Corynebacterium glutamicum*. *Gene*, 145, 69–73.

Simon, R., Priefer, U. & Pühler, A. (1983) A broad host range mobilization system for in vivo genetic engineering: transposon mutagenesis in gram negative bacteria. *Bio/Technology*, 1, 784–791.

Snow, S., Bacon, E., Bergeron, J., Katzman, D., Wilhelm, A., Lewis, O. et al. (2020) Transcript decay mediated by RNase III in *Borrelia burgdorferi*. *Biochemical and Biophysical Research Communications*, 529, 386–391.

Spanka, D.-T. & Klug, G. (2021) Maturation of UTR-derived sRNAs is modulated during adaptation to different growth conditions. *International Journal of Molecular Sciences*, 22, 12260.

Spanka, D.-T., Reuscher, C.M. & Klug, G. (2021) Impact of PNPase on the transcriptome of *Rhodobacter sphaeroides* and its cooperation with RNase III and RNase E. *BMC Genomics*, 22, 106.

Srivastava, A.K. & Schlessinger, D. (1990) Mechanism and regulation of bacterial ribosomal RNA processing. *Annual Review of Microbiology*, 44, 105–129.

Storz, G., Vogel, J. & Wassarman, K.M. (2011) Regulation by small RNAs in bacteria: expanding frontiers. *Molecular Cell*, 43, 880–891.

Vogel, J., Argaman, L., Wagner, E.G.H. & Altuvia, S. (2004) The small RNA IstR inhibits synthesis of an SOS-induced toxic peptide. *Current Biology*, 14, 2271–2276.

Westphal, H. & Crouch, R.J. (1975) Cleavage of adenovirus messenger RNA and of 28S and 18S ribosomal RNA by RNase III. *Proceedings of the National Academy of Sciences of the United States of America*, 72, 3077–3081.

Whitehead, N.A., Barnard, A.M., Slater, H., Simpson, N.J. & Salmond, G.P. (2001) Quorum-sensing in gram-negative bacteria. *FEMS Microbiology Reviews*, 25, 365–404.

Zahn, K., Inui, M. & Yukawa, H. (2000) Divergent mechanisms of 5′ 23S rRNA IVS processing in the alpha-proteobacteria. *Nucleic Acids Research*, 28, 4623–4633.

SUPPORTING INFORMATION

Additional supporting information can be found online in the Supporting Information section at the end of this article.

How to cite this article: Börner, J., Friedrich, T. & Klug, G. (2023) RNase III participates in control of quorum sensing, pigmentation and oxidative stress resistance in *Rhodobacter sphaeroides*. *Molecular Microbiology*, 00, 1–19. Available from: https://doi.org/10.1111/mmi.15181